AD-756 912

AN EXPERIMENTAL STUDY OF THE PRESSURE DISTRIBUTION IN BURNING FLAWS IN SOLID PROPELLANT GRAINS

Harold R. Jacobs, et al

Utah University

Prepared for:

Air Force Rocket Propulsion Laboratory

October 1972

AFRPL-TR-72-108

AD759912

AN EXPERIMENTAL STUDY OF THE PRESSURE DISTRIBUTION IN BURNING FLAWS IN SOLID PROPELLANT GRAINS

Final Report Task I
Submitted to the

Air Force Rocket Propulsion Laboratory
Contract #FO 4611-71-C-0031

October 1972

AFRPL-TR-72-108
UTEC DO 72-130

DEPARTMENT OF MECHANICAL ENGINEERING

UNIVERSITY OF UTAH
SALT LAKE CITY, UTAH 84112

AN EXPERIMENTAL STUDY OF THE PRESSURE DISTRIBUTION IN BURNING FLAWS IN SOLID PROPELLANT GRAINS

Final Report Task I
Submitted to the

Air Force Rocket Propulsion Laboratory
Contract #FO 4611-71-C-0031

October 1972

AFRPL-TR-72-108
UTEC DO 72-130

Principal Investigators

H. R. Jacobs
M. L. Williams

Graduate Research Assistant

D. B. Tuft

Security Classification

DOCUMENT CONTROL DATA - R & D

(Security classification of title, body of abstract and indexing annotation must be entered when the overall report is classified)

1. ORIGINATING ACTIVITY (Corporate author)	2a. REPORT SECURITY CLASSIFICATION
University of Utah College of Engineering Salt Lake City, Utah	Unclassified 2b. GROUP

3. REPORT TITLE

An Experimental Study of the Pressure Distribution in Burning Flaws in Propellant Grains

4. DESCRIPTIVE NOTES (Type of report and inclusive dates)

Final Report Task I March 15, 1971 - August 15, 1972

5. AUTHOR(S) (First name, middle initial, last name)

Harold R. Jacobs, Max L. Williams, Dean B. Tuft

6. REPORT DATE	7a. TOTAL NO. OF PAGES	7b. NO. OF REFS
October 1972	64	13

8a. CONTRACT OR GRANT NO.	9a. ORIGINATOR'S REPORT NUMBER(S)
b. PROJECT NO.	UTEC DO 72-130
c.	9b. OTHER REPORT NO(S) (Any other numbers that may be assigned this report)
d.	

10. DISTRIBUTION STATEMENT

This Document is approved for Public Release
Distribution Unlimited

11. SUPPLEMENTARY NOTES	12. SPONSORING MILITARY ACTIVITY
Details of illustrations in this document may be better studied on microfiche.	AFRPL/Edwards Air Force Base, California

13. ABSTRACT

Cracks or flaws in solid propellant grains have been responsible for the failure of many rocket motors and there has been much concern in the solid propellant rocket industry as to the extent that flaws could contribute to catastropic failure.

This study was conducted to determine experimentally what the pressure distribution in a solid propellant debond would be after the burning had propagated into it. The bulk of the work was experimental with the results being compared to a computer solution for flow in a variable area duct with mass addition. Results are given for three separate debond angles at several different chamber pressures.

The results lie well within the range of experimental error for the type of instrumentation and apparatus used to make the measurements and support the theory very well. From these experiments it is reasonable to conclude that a one-dimensional flow model will predict pressures in propellant flaws.

With a knowledge of what the pressure distribution will be within a burning flaw, predictions can be made as to the probability of a flaw or crack contributing to catastrophic failure.

DD FORM 1 NOV 65 1473

Security Classification

14. KEY WORDS	LINK A		LINK B		LINK C	
	ROLE	WT	ROLE	WT	ROLE	WT
Propellant						
Combustion						
Flaws						
Cracks						
Debonds						
Pressure Distributions						
Experimental						
Numerical						

TABLE OF CONTENTS

LIST OF TABLES AND FIGURES

NOMENCLATURE

A	cross-sectional area of duct
Br	non-dimensional blowing rate
C_p	constant pressure specific heat
C	burning rate coefficient
D	propellant density
ϵ	roughness height for sand-roughened pipes
f	plane wall friction factor
G	variable defined as $2(\gamma-1)T_0R/\gamma$
H	variable to correct friction factor for burning
h	specific enthalpy of gas
h_r	reference value of specific enthalpy used in a linear approximation of the relationship between enthalpy and temperature
M	Mach number
$\dot{m}$	mass flow rate
N	exponent in burning rate law
P	pressure at x
P_r	arbitrary reference pressure
P_0	stagnation pressure
$\bar{P}$	non-dimensional pressure defined as P/Pr
R	universal gas constant
Re	Reynolds number based on hydraulic diameter
r_b	propellant burning rate

S	total surface area $S_b + S_n$
T	temperature at x
T_o	stagnation temperature
u	gas velocity at x
U_s	gas velocity at boundary layer of a flat plate
V_w	normal gas velocity at wall
x	distance along debond measured from tip
y	debond width at x
γ	ratio of specific heats
ξ	variable defined as $(\bar{p}^2 + G^2\eta^2)^{\frac{1}{2}}$
μ	viscosity of gas
η	variable directly proportional to mass flux and defined as $\dot{m}/APr$
ρ	gas density
ρ_s	gas density in boundary layers of flat plate
τ_w	wall shear stress

Subscripts

b	conditions at a burning wall
N	conditions at a non-burning wall
r	reference value
w	conditions at the wall

INTRODUCTION

Flaws or cracks in solid propellant grains have been responsible for the failure of many rocket motors. Thus, there has been much concern as to when and why such flaws might propagate to the extent that they could contribute to catastrophic failure (1,2). Considerable work has been conducted in an attempt to analyze the factors which create cracks or debonds in solid propellants (3,4). Among this work is a method to radiographically detect flaws before the motor is fired (5). However, even the knowledge that the propellant grain is flaw free before firing is no assurance that flaws will not form after the motor is fired due to internal pressurization.

Much of the early work dealing with propellant cracks was carried out to determine if burning would propagate into a crack existing in a solid propellant grain (6,7). The results indicated definitely burning would propagate into cracks or debonds and that the rate at which the flame would propagate increased with chamber pressure.

Before firing, defects in propellants are formed in areas of stress concentration caused by geometry and thermal expansion. Thermal effects arise when the propellant is cast into the motor casing and placed in an oven to cure at temperatures between 130°F and 160°F depending on the type of propellant. After the curing period the motor is allowed to cool to room temperature and stresses are formed due to the difference in thermal expansion coefficients of the casing and the propellant. For casings made of fiberglass the thermal stresses are somewhat relieved due to flexure of the casing whereas steel casings do not yield as easily and larger stresses are encountered.

After the motor is fired, cracks can form due to the developed chamber pressure. The increased chamber pressure simply increases the stresses above those that existed in the unfired state (1). Flaws formed before or after ignition normally originate in regions of geometric stress concentration such as the tip of the star pattern. Flaws existing at the tip of the star pattern are extremely critical since their propagation path to the casing is minimum. Tests have been conducted at Thiokol Chemical Corporation, Utah Division, to determine the effects of cracks that exist near the tip of the star pattern (2). The result is usually propagation of the crack directly outward to the motor casing along the minimum length path.

On the microscopic level it is believed that cracks occur due to an adhesive failure between the binder (or fuel) and the oxidizing agent. Once the adhesion between these particles and the fuel has failed, small pockets are formed around the oxidizing agent particles and stress concentration factors of approximately three are experienced by the material. These microscopic flaws readily propagate to become finite cracks. Once a crack is formed, it is probable that ignition will occur within it as soon as it is reached by the burning surface. When this occurs, it is of importance to know whether the pressures developed by the combustion within the crack are sufficient to make the crack propagate or whether the flaw will merely add to the effective burning surface area of the motor.

In order to study the pressures developed in a burning flaw, it is necessary to develop a qualitative feeling for the governing parameters. This includes a knowledge of what the flow will look like and what parameters will affect it. If the exit cross-sectional

area of the crack is small compared to its burning area, the velocity of the gaseous effluent will be much larger than that external to the flaw and the flow will be directed outward with no flow into the crack. If the exit area is larger, there may be some partial invasion of the flaw by the external flow. Thus, the critical parameters which effect the flow in the flaw and, hence, the pressure are the propellant properties, main chamber pressure, defect geometry, main chamber gas velocity, propellant burning rate, and fracture propagation velocity. With a knowledge of these governing parameters, one is ready to study the pressure distribution within the flaw.

It is the main concern of this study to determine experimentally what the pressure distribution will be in a propellant debond once the burning has propagated into it and to compare the results with a one-dimensional quasi-steady flow theory developed to predict pressures in burning propellant flaws. A debond configuration was chosen to be studied basically because of ease of instrumentation. The results for the debond configuration are not totally unrelated to those for a crack, however. The debond is simply a crack with propellant on one side and the motor casing on the other. Where the crack has two burning surfaces, the debond has only one which makes pressure measurements along the non-burning surface possible without disturbing the flow pattern. Results of these measurements are compared to the predicted values as calculated using basic compressible flow theory and a computer model developed for cracks or debonds in Reference 8. Once the validity of the predicted pressure values for debonds is established, it will be a good assumption to assume the theory holds true for cracks as well.

ONE-DIMENSIONAL ANALYSIS OF A BURNING DEBOND WITH FRICTION AND MASS ADDITION

The following analysis is based on the assumption of quasi-steady state phenomena. This assumption can be justified on the basis that the propellant burning rate is much slower than will be the velocity of the gaseous effluent. Also, if mechanical propagation of the crack is encountered, the quasi-steady state assumption will hold if the velocity of mechanical propagation is much slower than the gaseous velocity or if the defect remains stable for a length of time and then propagates to a new stable geometry which is instantaneously ignited. Thus, the following analysis will be to determine the instantaneous pressure distribution within a burning propellant debond.

The governing equations for the state of the effluent gas and the basic geometrical configuration are given below:

Continuity	$\dot{m} = \rho u A$	(1)
Equation of state	$P = \rho R T$	(2)
Energy	$h + u^2/2 = h_o$	(3)
Heat capacity	$h - h_r = C_p T$	(4)

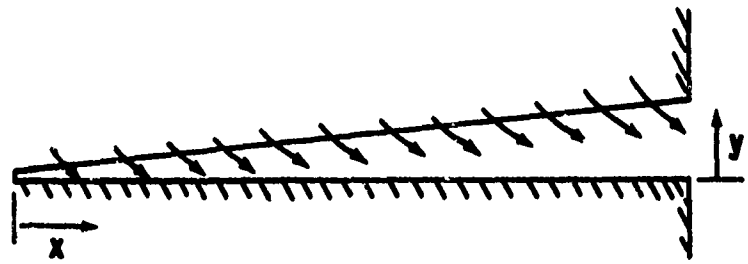

The basic assumptions include steady one-dimensional adiabatic flow, mass addition at constant enthalpy and negligible kinetic energy, and constant specific heat and viscosity. The assumption of mass addition at constant enthalpy and negligible kinetic energy is reasonable if the combustion zone is assumed infinitesimally thin and at the surface. This is a good assumption for most burning surfaces. The assumption of constant specific heat and viscosity simply implies that there is no chemical reaction taking place after the gas is added to the stream. Adiabatic flow is also a good assumption for solid propellant grains which release considerable energy and are very poor thermal conductors.

The momentum equation for one dimensional flow is:

$$\frac{P}{2}\frac{dS}{dx}\frac{dy}{dx} - \frac{d}{dx}(AP) - \tau_{wb}\frac{dS_b}{dx} - \tau_{wn}\frac{dS_n}{dx} = \frac{d}{dx}(\dot{m}u) \qquad (5)$$

where A = cross-sectional area; dS_b/dx = change in surface area at burning wall per change in x; and dS_n/dx = change in surface area at a non-burning wall per change in x. The quantity dy/dx is assumed small to insure the one dimensionality of the flow and the x component of momentum of the mass element, $\dot{m}$, added over the length dx is assumed negligible due to the assumption of normal burning.

For a debond the variation of flow area and differential surface area with x are of the form:

$$A = y$$
$$dS_b = dS_n = dx \qquad (6)$$

The momentum equation contains two types of wall shear stress-shear at the burning wall, τ_{wb}, and shear at the non-burning wall, τ_{wn}. Both types of wall

shear stress can be written in the form:

$$\tau_w = f \rho \frac{u^2}{2} \tag{7}$$

where the friction factor f_n for the non-burning wall is a function of surface roughness and Reynolds number. The friction factor f_b for a burning wall is dependent on Reynolds number and the mass addition rate which tends to blow the boundary layer away from the wall thus reducing the wall shear stress. Reference 9 has reported a correlation between friction factor for external flow with pressure gradient and non-dimensional blowing rate, B_R, where

$$B_r = \frac{\rho_w V_w}{\rho_s U_s} \sqrt{Re_x} \tag{8}$$

The problem of flow in a debond more closely resembles pipe flow than boundary layer flow and it would seem more reasonable to base Reynolds number on hydraulic diameter rather than distance from the leading edge. Doing this the expression for Reynolds number becomes:

$$Re = \frac{2yu\rho}{\mu} \tag{9}$$

For one-dimensional flow $\rho_w = \rho_s = \rho$ and the normal velocity at the wall, V_w, can be evaluated by considering a differential wall length dx. Thus

$$\dot{dm} = \rho V_w \, dx \tag{10}$$

Combining Equations 10 and 8 we obtain

$$B_r = \frac{1}{u} \frac{\dot{dm}}{dx} \sqrt{Re} \tag{11}$$

The earlier mentioned correlation presented in Reference 9 may be approximated to obtain the following form for the mass addition friction factor in terms of the plane wall friction factor f:

$$f_b = Hf \tag{12}$$

where

$$H \simeq \frac{1}{2}\left[\frac{1}{B_r + 1.0} + \frac{1}{5^{B_r/4}}\right] \tag{13}$$

For turbulent flow a similar type of correlation between f_b and f exists as given in Reference 10.

Since the case at hand closely approximates pipe flow, the friction factors can be found by the use of a Moody diagram for rough pipes. The relationship for laminar flow is

$$f = \frac{64}{Re} \tag{14}$$

For turbulent flow the friction factor for a rough pipe depends on surface roughness and Reynolds number. Specific values of f for turbulent flow can vary between approximately 0.07 and 0.01 depending on the degree of turbulence and roughness. Several equations have been proposed to characterize the behavior of f for turbulent flow. Such an equation has been developed for sand roughened pipes in Reference 11 and has the following form:

$$\frac{1}{\sqrt{f}} = 1.14 - 0.86 \ln \frac{\varepsilon}{y} \tag{15}$$

where ε is the roughness height for sand roughened-pipes and can be compared to the particle size of the oxidizing agent in a solid propellant.

Substituting Equations 6, 7, and 12 into the general momentum equation one obtains

$$y \frac{dP}{dx} - f\rho u^2 \left(\frac{1+H}{2}\right) = \frac{d}{dx}(\dot{m}u) \tag{16}$$

where f and H are determined by Equations 11, 13, 14, and 15.

The problem is now defined in terms of five basic equations--energy, continuity, momentum, heat capacity, and the equation of state. These five equations are expressed in terms of seven basic variables--h, T, y, u,

P, ρ, and $\dot{m}$. It is now possible to express any one parameter as a function of any other two.

If we use the perfect gas relation, Equation 2, the property relation, Equation 4, and the continuity relation, Equation 1, to eliminate ρ, u, and h from the momentum and energy equations, we arrive at

$$\bar{p}\frac{dy}{dx} - \frac{d}{dx}(y\bar{p}) - \frac{f}{2\bar{p}}\,T\eta^2R\,(1+H) = \frac{d}{dx}\left(\frac{y}{\bar{p}}\,T\eta^2R\right) \tag{17}$$

and

$$(\gamma - 1)\,(T\eta^2R) + (2\bar{p}^2\gamma)\,(T\eta^2R) - 2T_0\bar{p}\gamma\eta^2\,R = 0 \tag{18}$$

where

$$\bar{p} = P/P_r \text{ and } \eta = \dot{m}/P_rA$$

Solution of Equation 18 by the quadratic formula yields

$$T\eta^2R = \frac{-\bar{p}^2 \pm \bar{p}\gamma\,(\bar{p}^2 + G^2\eta^2)^{\frac{1}{2}}}{\gamma-1} \tag{19}$$

where

$$G = 2(\gamma-1)T_0\,R/\gamma$$

is a constant parameter of the propellant. Price (12) has shown that of the two signs possible in Equation 19 only the plus sign has physical significance since the minus sign corresponds to removal of mass in an unmixing process which leads to a decrease in entropy. If we define a new variable:

$$\xi = (\bar{p} + G^2\eta^2)^{\frac{1}{2}}$$

and combine Equation 19 with Equation 17 after some rearrangement we obtain

$$\frac{d\bar{p}}{dx} = \frac{\gamma\xi}{y(\xi - \gamma\bar{p})}\left((\xi-\bar{p})\left[\frac{f}{2}(1+H) + \frac{dy}{dx}\right] + \frac{G^2\eta}{\xi}\left[\eta_0\bar{p}^N - \eta\frac{dy}{dx}\right]\right) \tag{20}$$

The burning rate of a propellant neglecting errosive burning may be represented by the empirical relation

$$r_b = CP^N \tag{21}$$

where r_b is the local recession rate of the burning wall and C and N are constants dependent upon the propellant. The local differential mass flux is then $d\dot{m} = Dr_b dx$ where D is the density of the solid. The local mass flux may now be integrated to obtain

$$\dot{m} = \int_0^{S_b} Dr_b dx + \dot{m}_o \tag{22}$$

where $\dot{m}_o$ indicates the presence of burning on the head end and has the value

$$\dot{m}_o = DC\, P_o^N\, A_o \tag{23}$$

Combining Equations 22 and 23 and the definition of the variable $\eta = \dot{m}/APr$, one obtains

$$\eta = \frac{\eta_o}{y}\left(\int_0^x \bar{p}^N\, dx + y_o\right) \tag{24}$$

where $\eta_o = DCP_o^{N-1}$

We may now solve for the pressure distribution, or equivalently $\bar{P}$, as a function of x by simultaneously solving the differential equation for $\bar{P}$ (Equation 20) and the integral equation for η (Equation 24).

In order to solve the governing equations, it is necessary to establish a boundary condition at the flow exit. If the flow is subsonic at the exit plane, then the pressure must be equal to the main chamber pressure, P_{CH}. If the flow is choked at the exit plane, the boundary condition must be Mach number equals one.

In terms of the variables defined earlier, the Mach number can be shown to be represented by the relationship

$$M^2 = \frac{(\xi - \bar{P})}{\bar{P}(\gamma - 1)} \tag{25}$$

A computer program has been devised to give the solution of the governing equations (8). This program will be used to provide theoretical results for comparison with the experimentally determined pressure distributions.

EXPERIMENTAL APPARATUS AND PROCEDURES

BASIC EQUIPMENT

A side view of the model used to experimentally simulate a burning debond with transducers in place is shown in Figure 1. The dimensions of the burning surface are three inches wide by four and one-half inches long. The propellant slab is 0.10 in. thick and can be seen as a thin layer on the lower half of the debond model in Figure 1. These dimensions were chosen basically to attempt to keep the amount of propellant burned in each test small while keeping the dimensions of the flaw on the same order as those that might exist in real motors. The angle of divergence of the debond model is variable with a maximum of just over five degrees. This allows the same model to be used to examine debonds with different angles of divergence. The transducers shown in Figure 1 are located at positions .19, 1.72, and 3.72 inches from the debond tip.

In order to simulate the externally imposed chamber pressure that exists in a rocket motor experiments were conducted in a combustion chamber which is shown in Figure 2. The chamber is approximately one foot in diameter and three feet long with a maximum working pressure of 1000 psi. Experiments were conducted with a range of simulated chamber pressures using both air and nitrogen to pressurize the chamber. The long narrow window on the side of the chamber made visual observation of the tests possible.

The narrow window in the chamber and the use of 0.25 inch thick plexiglas side pieces in the debond model allowed photographic visualization of the burning process. Pyrex glass was initially used for the side pieces, however, it did not work satisfactorily. The high

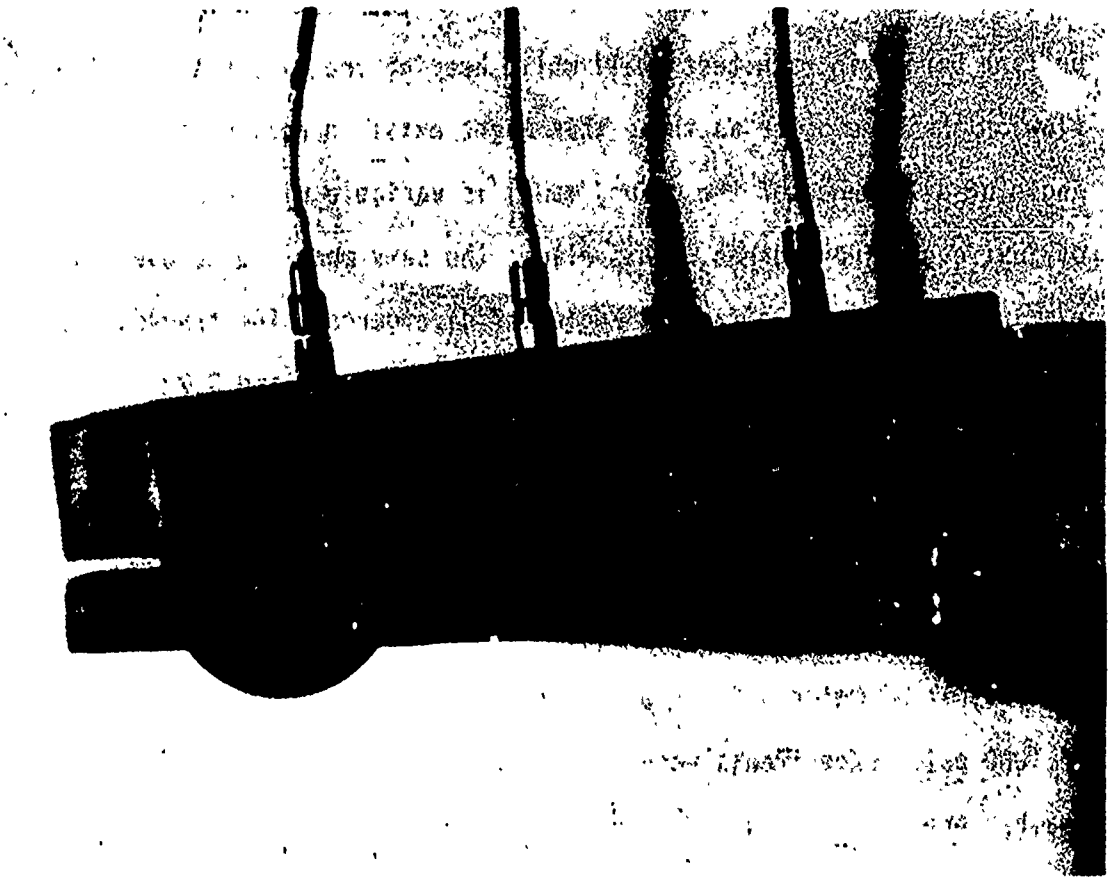

Figure 1. Debond model with transducers in place.

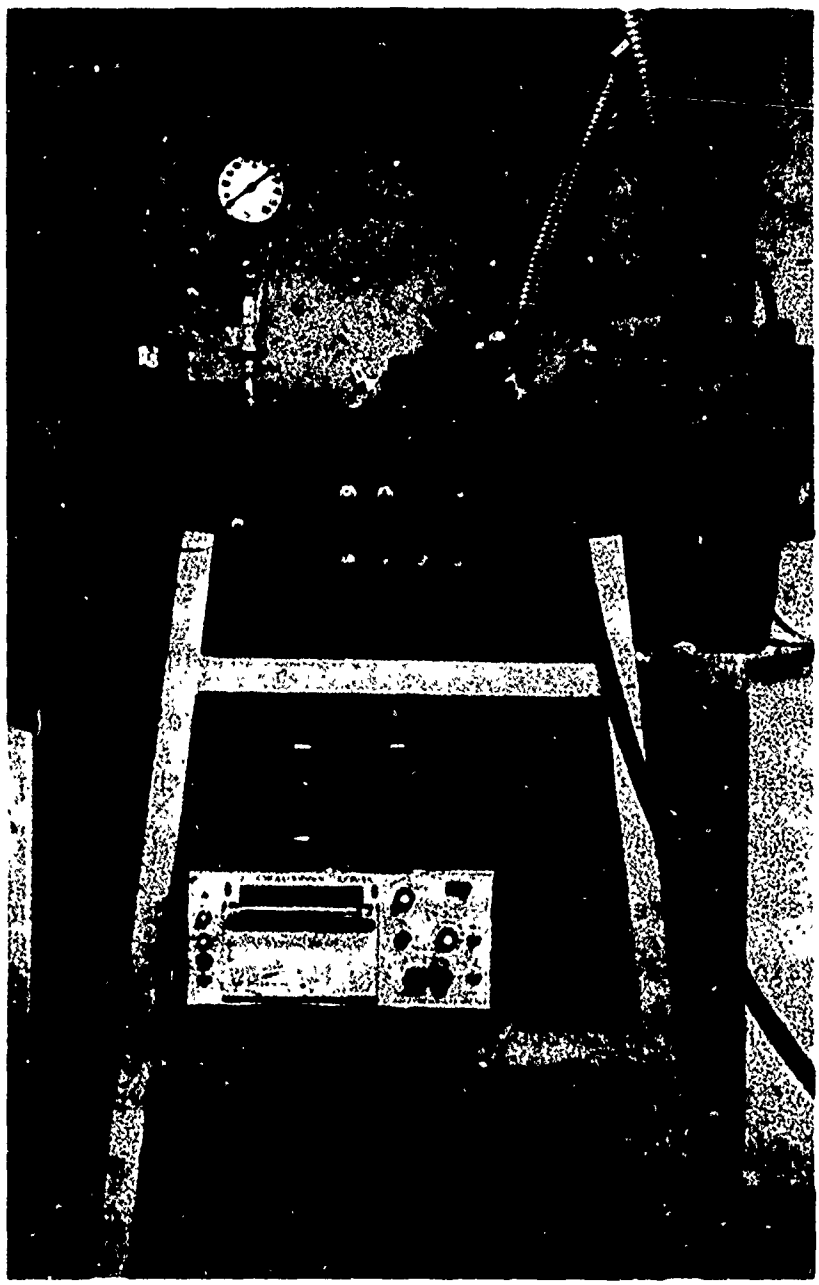

Figure 2. Combustion bomb and instrumentation

temperature of the burning propellant and the very rapid application of large amounts of heat caused the pyrex side pieces to crack. Plexiglass side pieces proved to work very well in place of the pyrex. The plexiglass side pieces were able to withstand the high temperature of the burning without melting away completely due to the very short duration of the burn and the ability of plexiglass to yield without fracture under thermal stress.

Motion pictures were obtained at 64 frames per second for several of the experiments using a Bolax 16-mm camera and high-speed infrared film. Typical pictures obtained from one run are shown in Figure 7. The photos shown are for the very first portion of the burn only. This is due to the fact that smoke building up within the chamber would obscure the view of the model after approximately 0.1 seconds in each run and it was impossible after that to see the burning through the smoke. The photos that were obtained for approximately the first tenth of a second were of acceptable quality. With these pictures one can obtain a good qualitative feeling for how well the ignition is occurring and how the propellant is burning with time for the first part of the burn. Since smoke had made visual recording of how the propellant was burning with time impossible, it was necessary to use those photos that were obtained for the initial portion of the burn to estimate when data could be reduced. It was necessary to reduce the data at a time when the geometry had not been changed significantly by burning.

As can be seen in Figure 2, two spring-operated pressure relief valves are attached to the combustion chamber. These valves were

used to attempt to regulate the pressure within the chamber. The regulation achieved by the use of the pressure relief valves was relatively poor at low chamber pressures due to their inability to maintain large enough flow rates. Also the combustion gases that were being exhausted through the valves were highly corrosive and required their frequent replacement. Although the chamber pressure was not held constant, the increase in pressure that was experienced by the chamber was recorded so that the exact chamber pressure at any instant was known.

INSTRUMENTATION

The pressure measurements were made at three locations along the debond and at one location on the pressure chamber using Kistler Model 603A quartz pressure transducers. A drawing of one of these transducers is shown in Figure 3 along with a cross-section of the mounting configuration used. The recessed style of mounting was chosen to protect the transducers from the extreme heat of the burning propellant (approximately 6000^{o}R). At the high temperatures encountered in these experiments, the seal on the transducers is very important. Even the slightest gas leaks can cause extremely high heat transfer rates which may damage the transducer. A stainless steel sleeve also shown in Figure 3 serves to provide the seal necessary to protect the instument. With this seal and a snug fit the transducer itself never experiences temperatures above its working maximum of 500^{o}F. The 1/16-inch connecting passage also helps protect the transducer by removing it from direct contact with the hot flowing gases while at the same time allowing adequate frequency response. With the use of the recessed mounting configuration and given the short duration of the

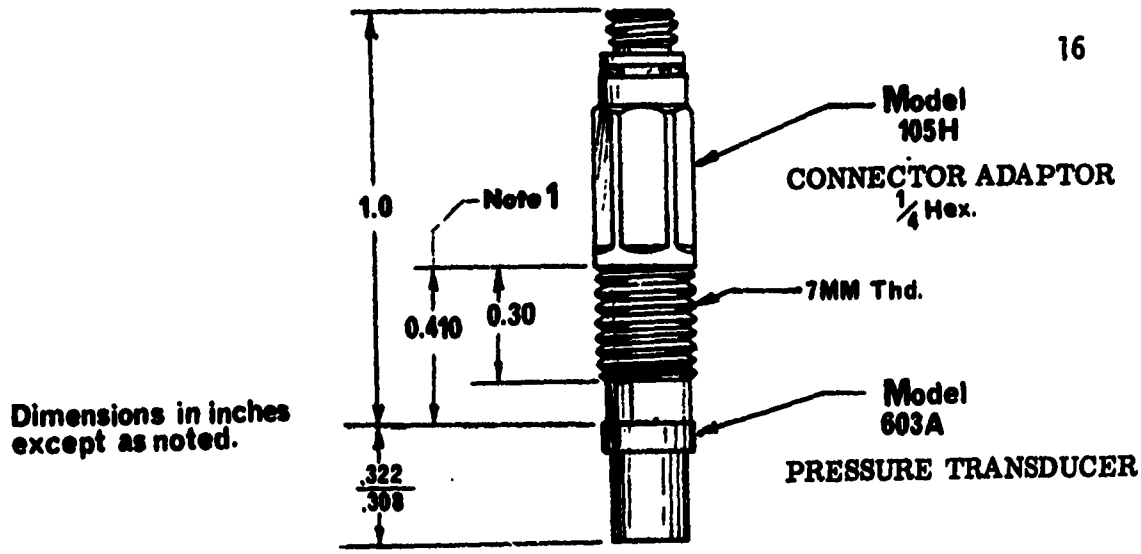

(a.) Transducer and Adaptor

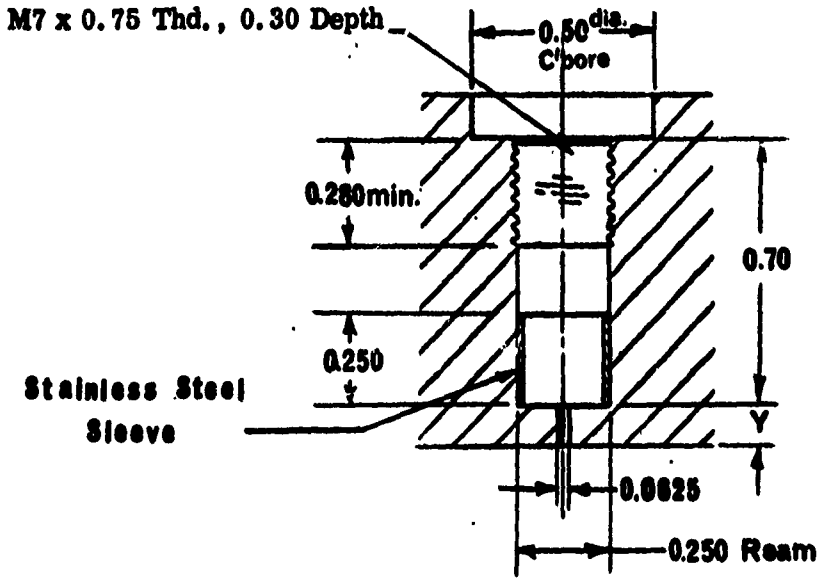

(b.) Recessed Mounting

Figure 3 Kistler Tranducer

burn, these transducers will withstand gas temperatures of well above $6000^{o}F$.

After a given number of tests the transducers were each checked against a dead weight tester to determine if there had been any damage from temperature effects. The check showed that the transducers had not been damaged by the tests.

The basic theory of operation of a quartz transducer begins with pressure applied to the diaphragm of the transducer which is converted to a force acting on the transducer crystal. This causes the transducer crystal to generate an electrical charge output which is proportional to the pressure input. The basic sensitivity of these instruments is "unit charge per unit pressure" and is expressed in picocoulombs per psi (pcb/psi). Because the output of the transducer is a high-impedance charge signal, a charge amplifier is required. The charge amplifier converts the high impedence charge signal from the transducers to a low impedence voltage or current signal required to drive the recording or display equipment.

The charge amplifier is a dc voltage amplifier with a capacitive feedback path from the low-impedence output circuit to the high-impedence input circuit. The output voltage which results from a charge signal input is returned to the input circuit through the feedback capacitor, in the direction to maintain the input circuit voltage at or near zero. Thus the net charge from the input circuit is stored in the feedback capacitor, producing a potential difference across it equal to the value of the charge divided by the value of

capacitance, and this potential difference determines the relationship of the output signal voltage to the input signal charge. The transfer characteristic or "gain" of the amplifier depends only on the value of the feedback capacitor (selected by a range switch) and the setting of a precision voltage divider (calibration factor dial), and is unaffected by time, temperature, or line voltage fluctuations (13).

The charge signal from the transducer is extremely sensitive to line capacitance or contaminants on the contact surface. For this reason only special low noise coaxial cables are suitable to transmit the signal from the transducer to the charge amplifier. Any stray capacitance such as dirt or moisture in the connectors will cause spurious signals due to the breakdown of the transducers' high insulation resistance by the contaminant. The manufacturer suggests that freon solvent, due to its excellent dielectric properties, and lint-free paper wipers are the best way to keep the connectors clean. Other solvents such as alcohol tend to contaminate insulators and should not be used.

For most applications the signal can be fed directly from the charge amplifier to the readout equipment without further amplification. The charge amplifiers do have a limited output capability and in some cases additional amplifiers are required to drive the readout equipment.

The equipment used for readout in these experiments was a B & F model 3006-DL ultraviolet oscillograph. This instrument utilizes light sensitive paper and a zenon lamp to produce a trace. The

oscillograph has a capacity of twelve channels, each channel requiring a galvanometer for operation. Only four channels were required for this work, however.

The galvanometers that were utilized here consist of simply a small mirror suspended by a coil of very fine wire. The deflection in the trace is achieved by the magnetic field applied to the coil when current is passed through it which subsequently causes rotation of the mirror in proportion to the magnitude of the applied magnetic field. It was found that the current output of the charge amplifiers is somewhat limited and was insufficient to drive the galvanometers full scale at the voltage levels encountered. Thus it was necessary to place an operational D. C. amplifier in line between each of the charge amplifiers and the oscillograph to provide the necessary current. For convenience, the amplifiers were chosen with a gain setting of unity in order that their current output capabilities could be taken advantage of without amplifying any noise that might exist in the system. A schematic of the instrumentation circuit for one channel is shown in Figure 4.

An ultra-violet recorder was chosen because the extreme transient nature of the tests required that the output device have a very fast writing speed and also a very high frequency response. The writing speed of the light sensitive recorder used is on the order of a maximum of 60,000 inches per second and the frequency response of the galvanometers that were chosen was at least 1000 Hertz. This combination of fast writing ability and quick response was more than adequate to record the events accurately without any appreciable lag.

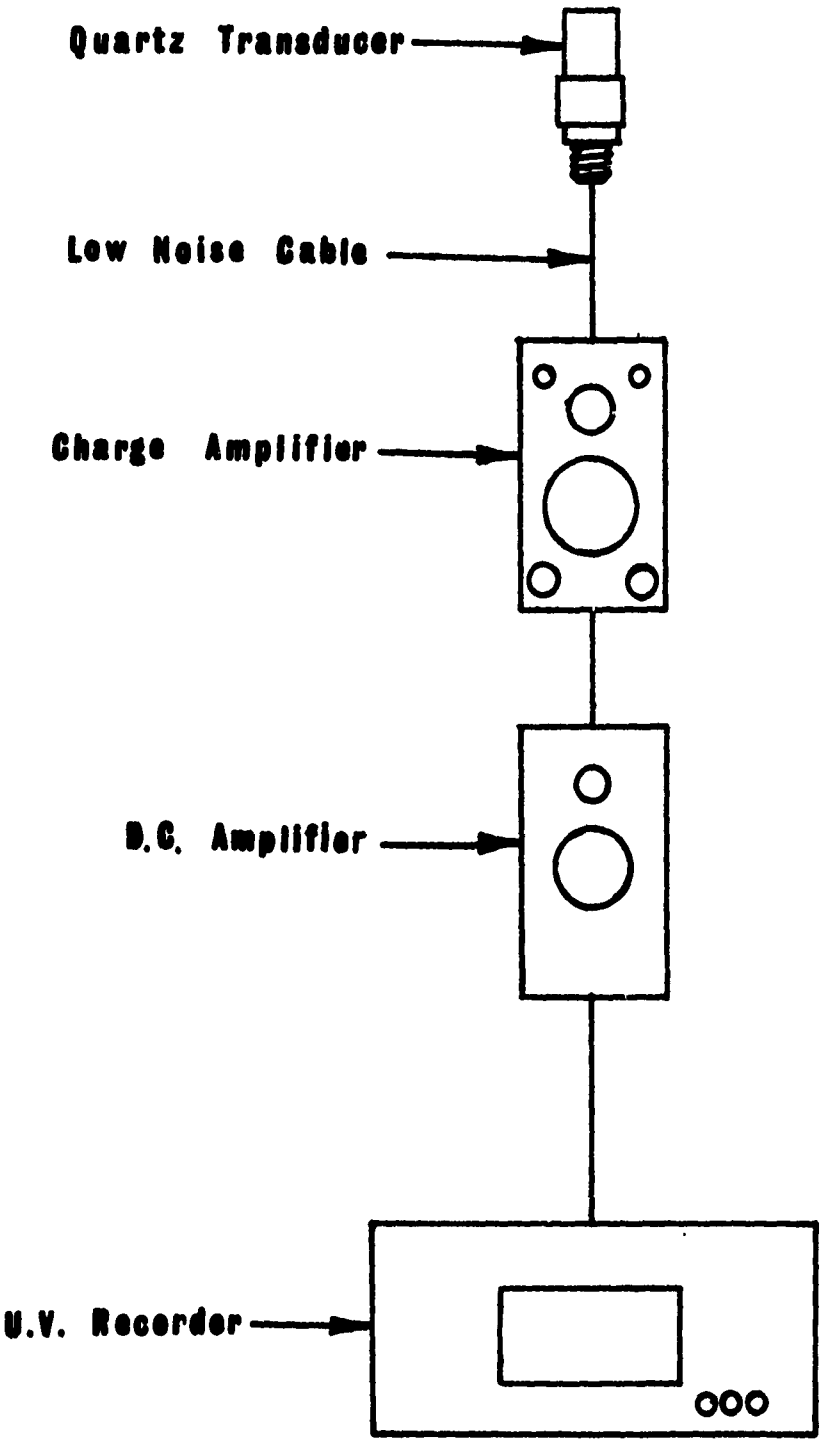

Figure 4 Instrumentation Circuit

In order that the ignition process be recorded correctly, it was required that the paper drive on the recorder be started just slightly before the ignition took place. This would be no problem to achieve manually for slow paper speeds, but at the faster speeds used it would mean wasting large amounts of light sensitive paper which was quite expensive. To save on paper and make the ignition simple a time-delay relay was incorporated in the ignition circuit. A single throw double-pole switch was used to start the paper drive and simultaneously energize a timed relay which was set to provide current to the ignition wire and an event marker on the oscillograph after approximately a two second delay. This circuit made it possible to begin the entire event by simply throwing a single switch. The ignition circuit is shown in block diagram form in Figure 5a and the wiring diagram is shown in Figure 5 b.

The paper drive was set at 4 inches per second and the paper was marked with vertical timing lines at 0.1 second intervals. The event marker made it possible to determine the time elapsed between ignition and the initial displacement of the recorder trace.

IGNITION OF A SOLID PROPELLANT SURFACE

As has been mentioned the surface of the propellant in the debond model was three inches wide and four and one-half inches long. In order that the tests be meaningful and comparable with the computer analysis, it was required that the entire surface be burning at the time of the pressure measurement. This made it necessary to ignite the propellant over the entire surface "instantaneously." The word

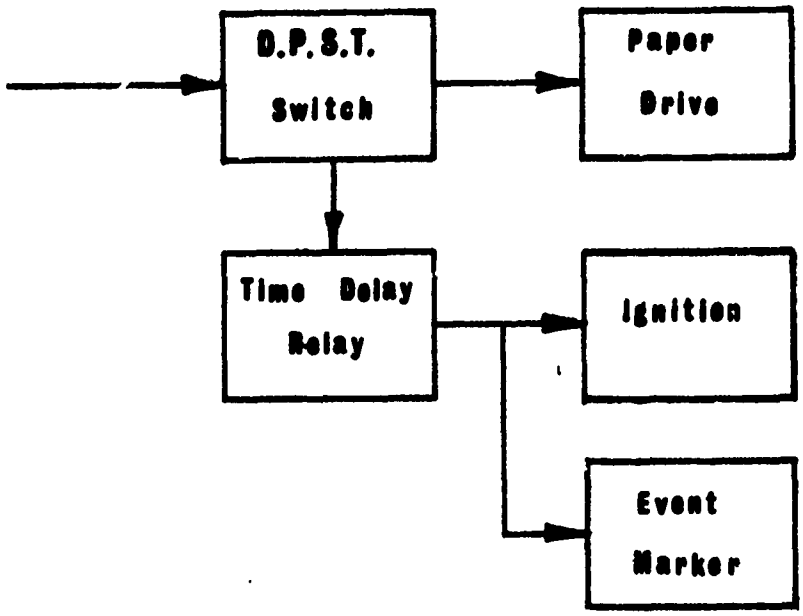

(a.) Block Diagram

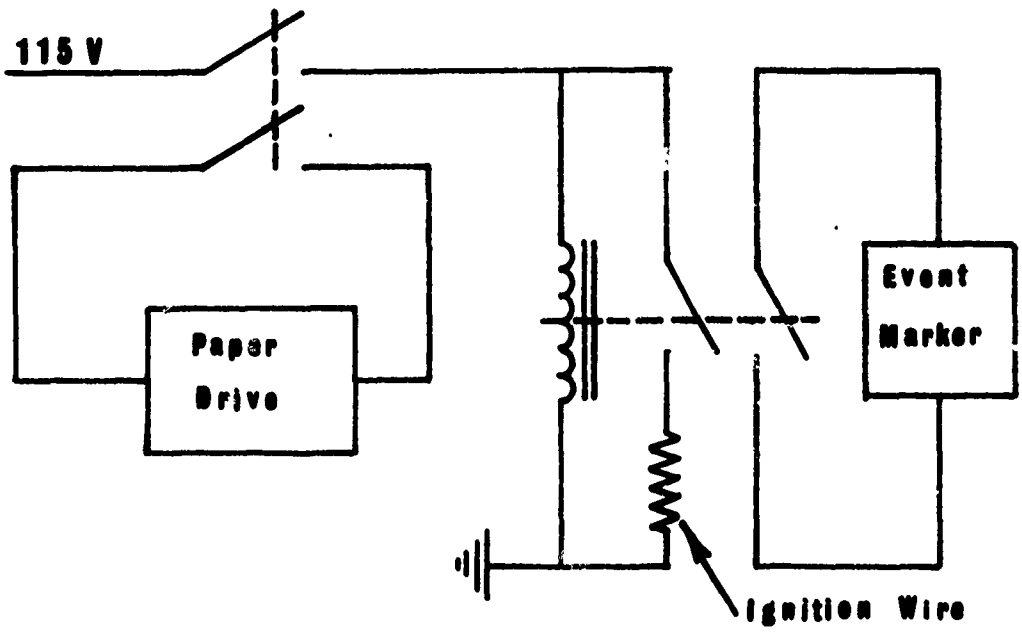

(b.) Wiring Diagram

Figure 5 Ignition Circuit

instantaneously being used to mean that the entire surface should be burning before any appreciable burning normal to the surface has occurred. The propagation rate of burning over a free surface is much faster than the burning rate normal to the surface and this effect is increased noticeably at higher pressures. Several methods were investigated to attempt to achieve suitable ignition over the entire surface.

The goal was to achieve very rapid ignition of the surface at atmospheric pressure so that the ignition under increased pressures could be safely assumed to approach that of instantaneous ignition over the entire surface.

Among the methods of achieving instantaneous ignition of a surface is that of painting the surface of the propellant with a mixture of red phosphorus powder and an organic binder such as common Duco cement. This method was among the first tried and did not give satisfactory results. The reason being perhaps that the red phosphorus which had been used had been exposed to moisture and had lost its flammability characteristics. The next method attempted was simply roughening the surface. While this did tend to make the flame spread more rapidly across the surface, the propagation rate of the burning was still not rapid enough to fulfill the requirement of instantaneous ignition.

Another common method of achieving rapid surface ignition is spreading a highly flammable powder over the surface. The first substance that was investigated was simply powdered propellant. The propellant powder ignited extremely fast but produced only enough heat to ignite the solid body of propellant in a few locations. The flash

of the propellant powder was on the order of the ignition speed that was being sought although it did not ignite the propellant properly. The problem was now to find a powder that would flash when ignited and produce enough heat to start the propellant burning everywhere.

A method to retain the heat produced by a powder that burns extremely fast is mixing iron filing or aluminum paint flake with the powder. Iron filings were mixed with both propellant powder and black gun powder and tested for ignition. Neither method seemed to work although the black powder gave better results than any of the method previously attempted. The iron filings used were quite coarse and perhaps if they were smaller, the test would have given better results.

It was finally discovered that metals such as titanium, zerconium, and magnesium when ground to very fine powders and mixed with an oxidizer will burn extremely fast and give off large amounts of heat at the same time. The powdered metals must have particle sizes on the order of thirty to fifty microns or smaller. The smaller the particles, the faster will be the burning rate and the smaller the time for heat transfer to the propellant. Of the many mixtures possible, it was found that a mixture of seventy per cent titanium and thirty per cent ammonium perchlorate powder worked very well. The titanium used had an average particle size of five microns and the ammonium perchlorate particles were fifteen microns on the average. Larger particles up to twenty or thirty microns average could be used with the same results.

The ignition procedure was then defined as follows. A very fine nichrome wire was attached to the surface of the propellant in a pattern as shown in Figure 6. On top of the wire and the propellant

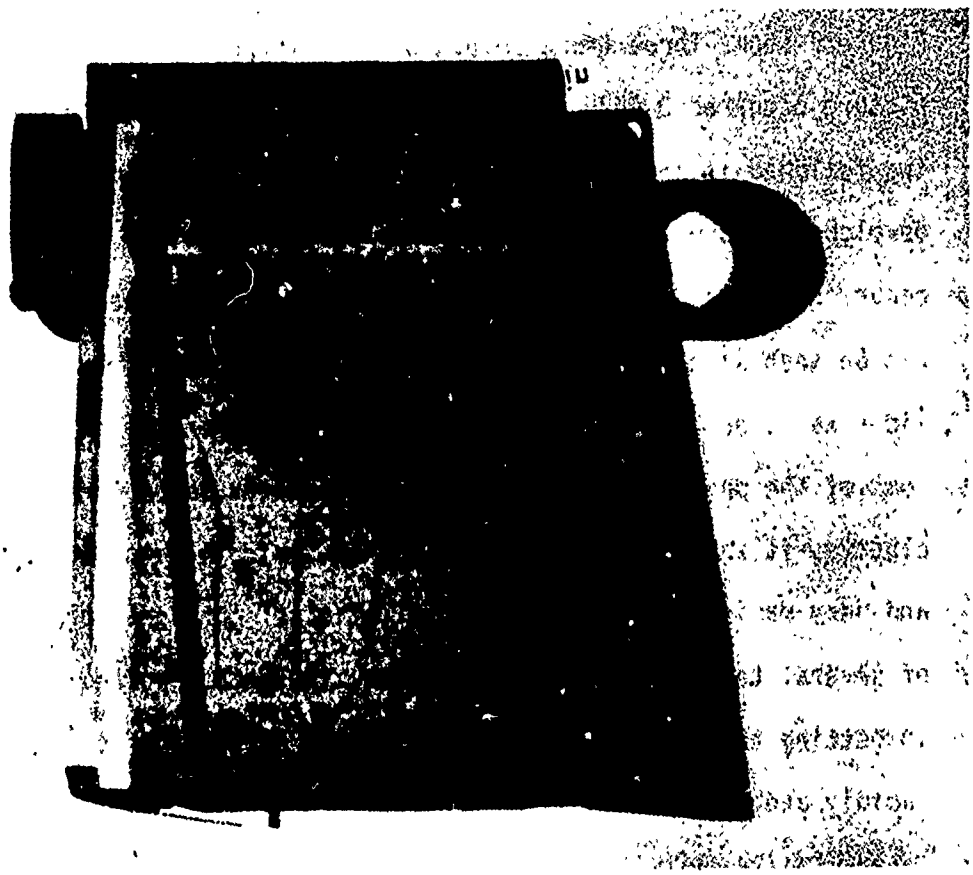

Figure 6. Lower half of debond model showing ignition wire

there was then spread a very fine layer of the aforementioned mixture of titanium ignition powder. It was very important that the powder be spread evenly over the entire surface so that the heat from the flash would reach every section of the surface evenly. With the wire and powder in place the debond model was ready for ignition.

Several trial tests were run and motion pictures taken to try to determine if the ignition was indeed as good as it appeared to be. Figure 7 shows three frames blown up from these pictures. The top picture occurred 0.0625 seconds after ignition contact and the other two followed in sequences of 1/64 of a second. The flow pattern developed in the top picture was the first evidence of burning to occur in the sequence. In the bottom picture the propellant slab can be seen with little sign of geometry change due to burning. The tip area is obscured by smoke and the ring section of the model in some of the photographs. Although the pictures taken were not conclusive, it seems that the propellant was being ignited quite evenly and very rapidly. From visual observation of the ignition phenomena of several tests, it was concluded that the method worked very well in getting the propellant ignited over the entire surface evenly and rapidly and also the ignition was very repeatable from test to test.

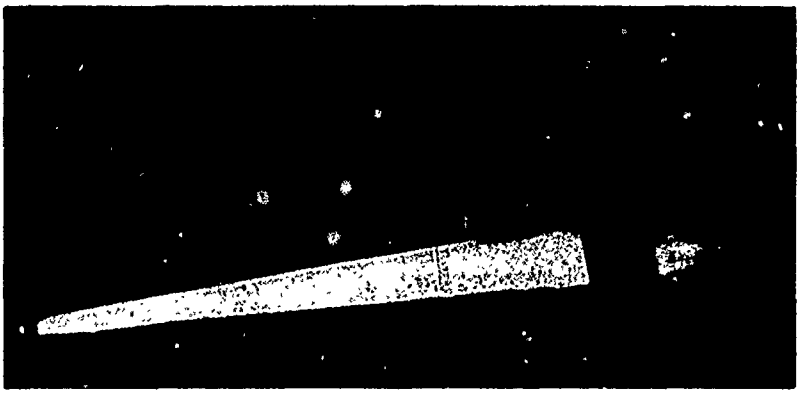

a) 0.0625 seconds after ignition contact

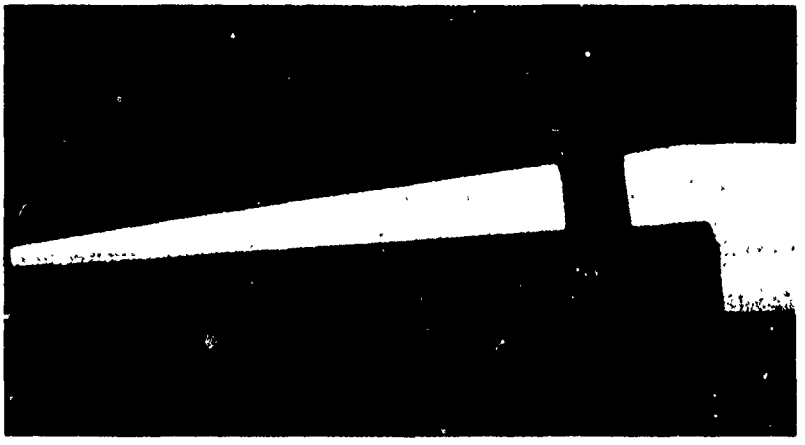

b) 0.078 seconds after ignition contact

c) 0.0935 seconds after ignition contact

Figure 7 Photos of a typical ignition sequence

DISCUSSION OF RESULTS

The experimental results are shown in Figures 8 through 14. Comparison with numerical solutions are indicated. Experiments were conducted for debond angles of 4.75 degrees and 3.17 degrees and 1.90 degrees and the data reduced at chamber pressure of 170, 245, 300, 332, 400, 550, and 600 psi. The data is plotted with an error band of $\pm$ ten per cent to give the reader an idea of the magnitude of the experimental error incurred in each case. The details of the geometries are given for each case along with the plot of the results.

The tip width specified in each case is a necessary geometrical consideration in order to eliminate the singularity that exists in the mathematical analysis for a tip width of zero. As can be seen trend of the curves predicted by the theory, the pressure approaches infinity asymptotically for small values of tip width and x close to zero. Since the pressure cannot logically be infinite at the tip and also to make a solution possible mathematically, it becomes necessary to assume a tip width other than zero. This assumption is valid on the basis that a truly sharp crack does not exist in nature. Determination of the tip width to be used is based somewhat on a knowledge of the configuration to be studied and an analysis of how the tip width will effect the theoretical pressure distribution within the debond.

The effect of a change in tip width on the predicted values of tip pressure and also pressure distribution is shown in Figure 15 for a typical debond configuration. As can be seen from the figure, the distribution of pressure within the flaw is little affected for varying tip widths below 0.001 of an inch and beyond a point approximately 0.6 inches away

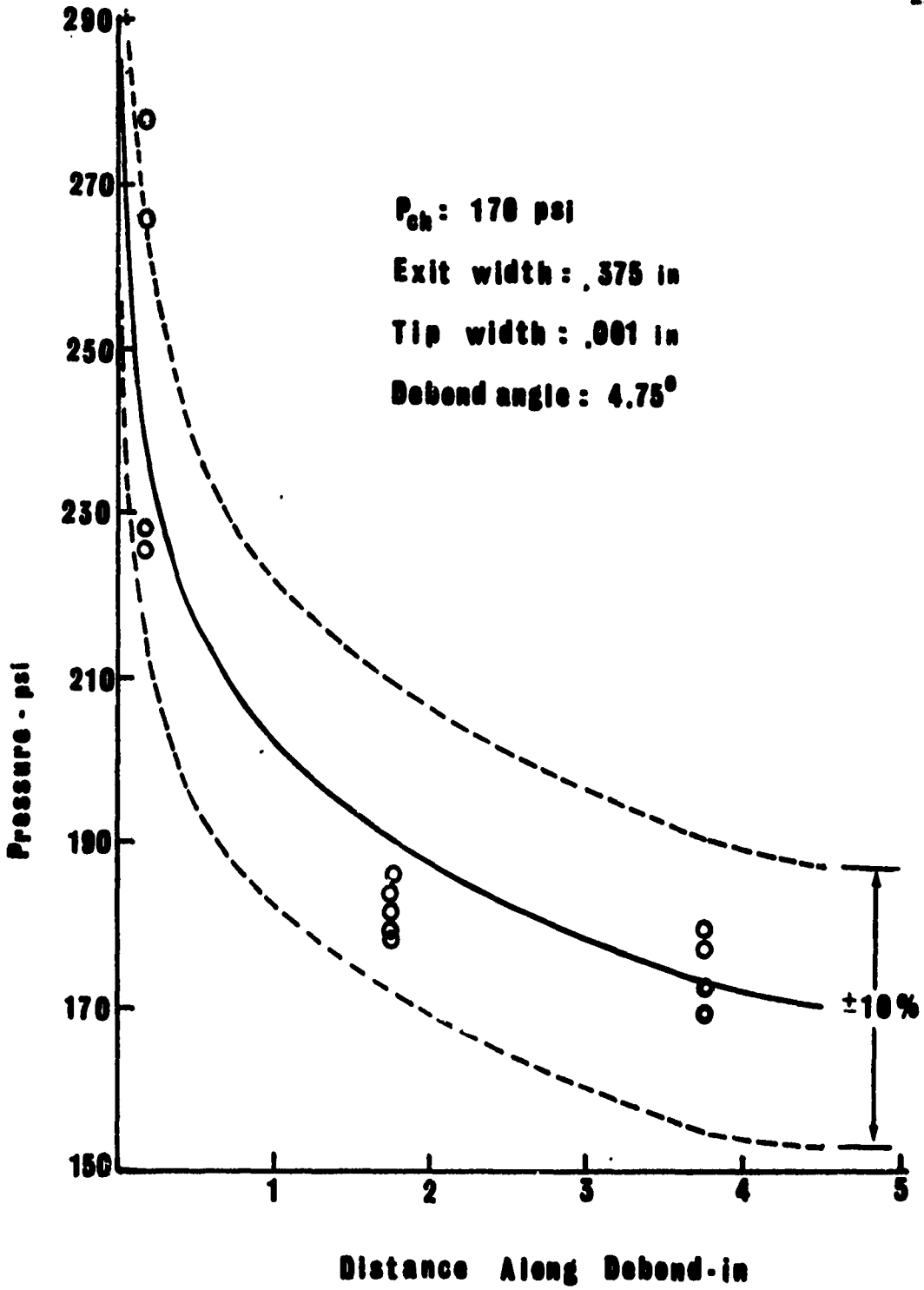

Figure 8 Pressure at x versus distance from tip

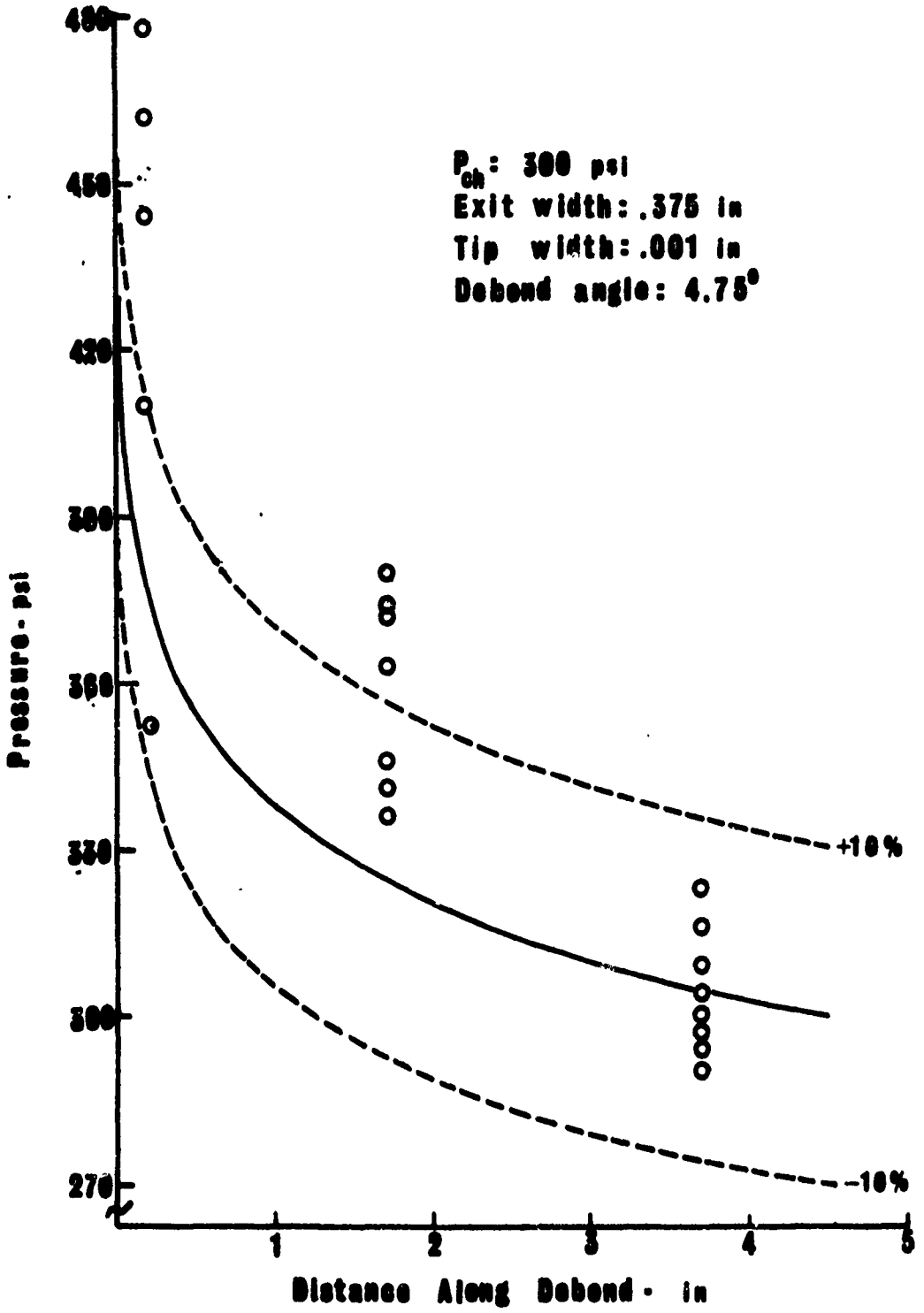

Figure 9 Pressure at x versus distance from tip

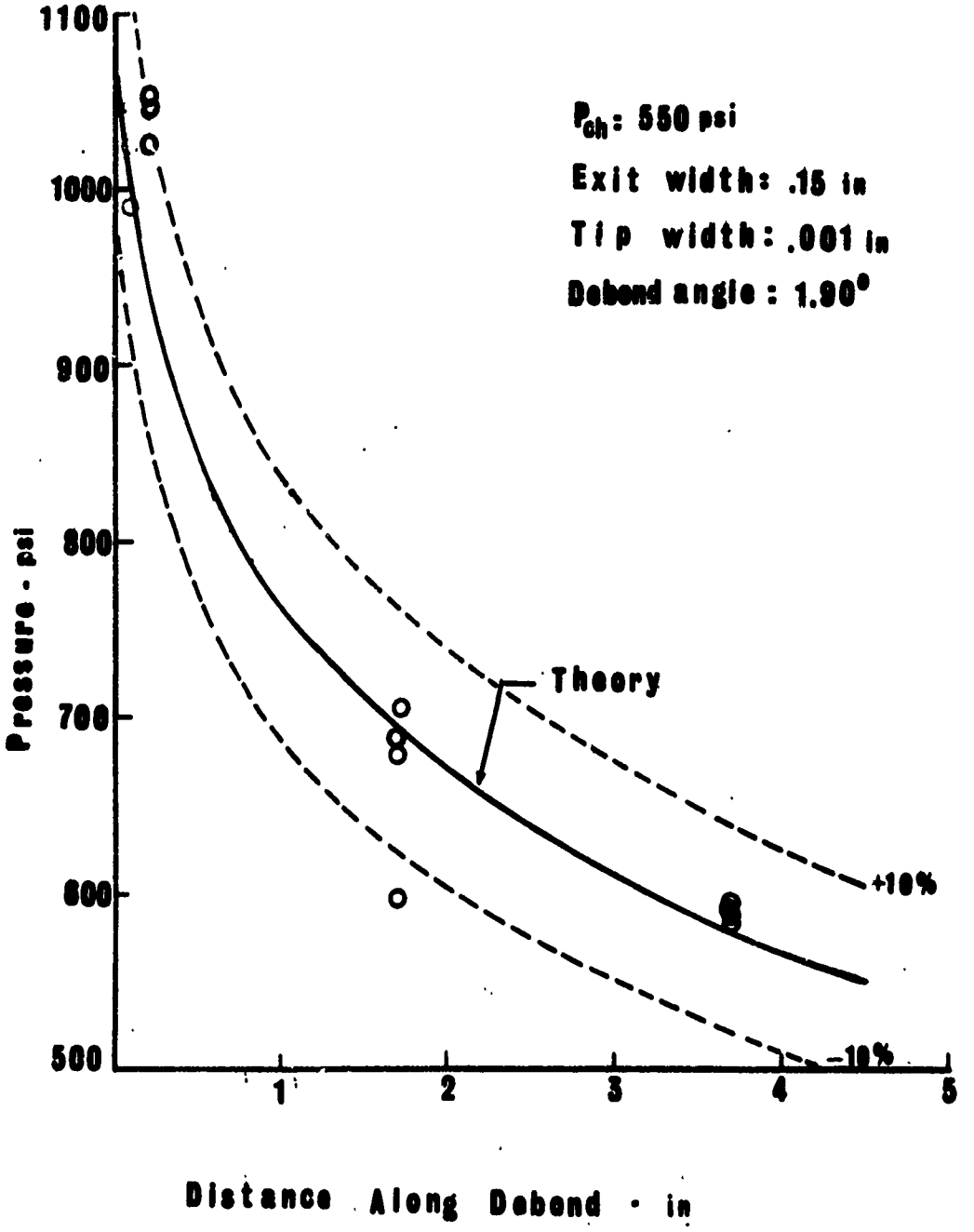

Figure 10 Pressure versus distance from tip

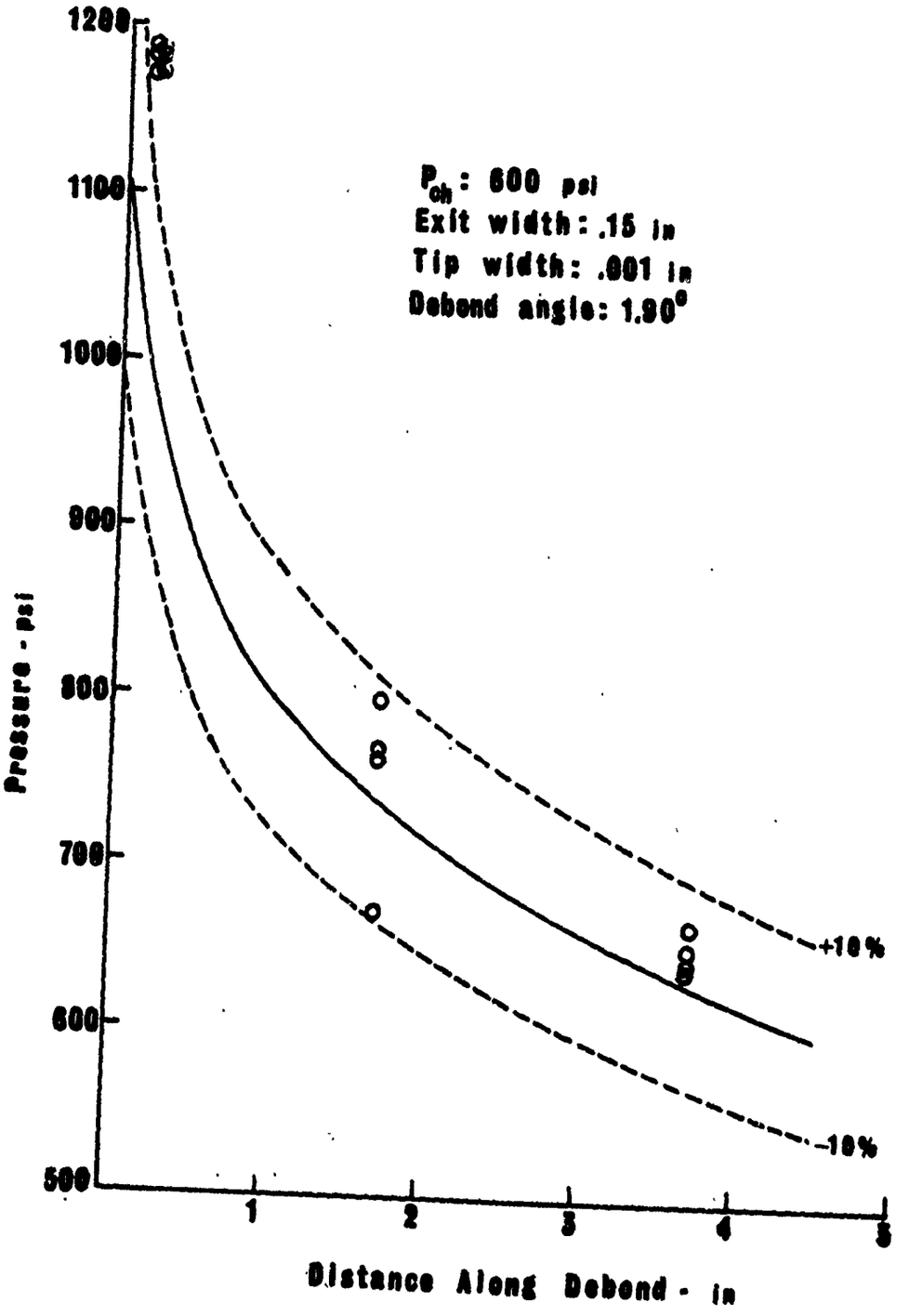

Figure 11 Pressure at x versus distance from tip

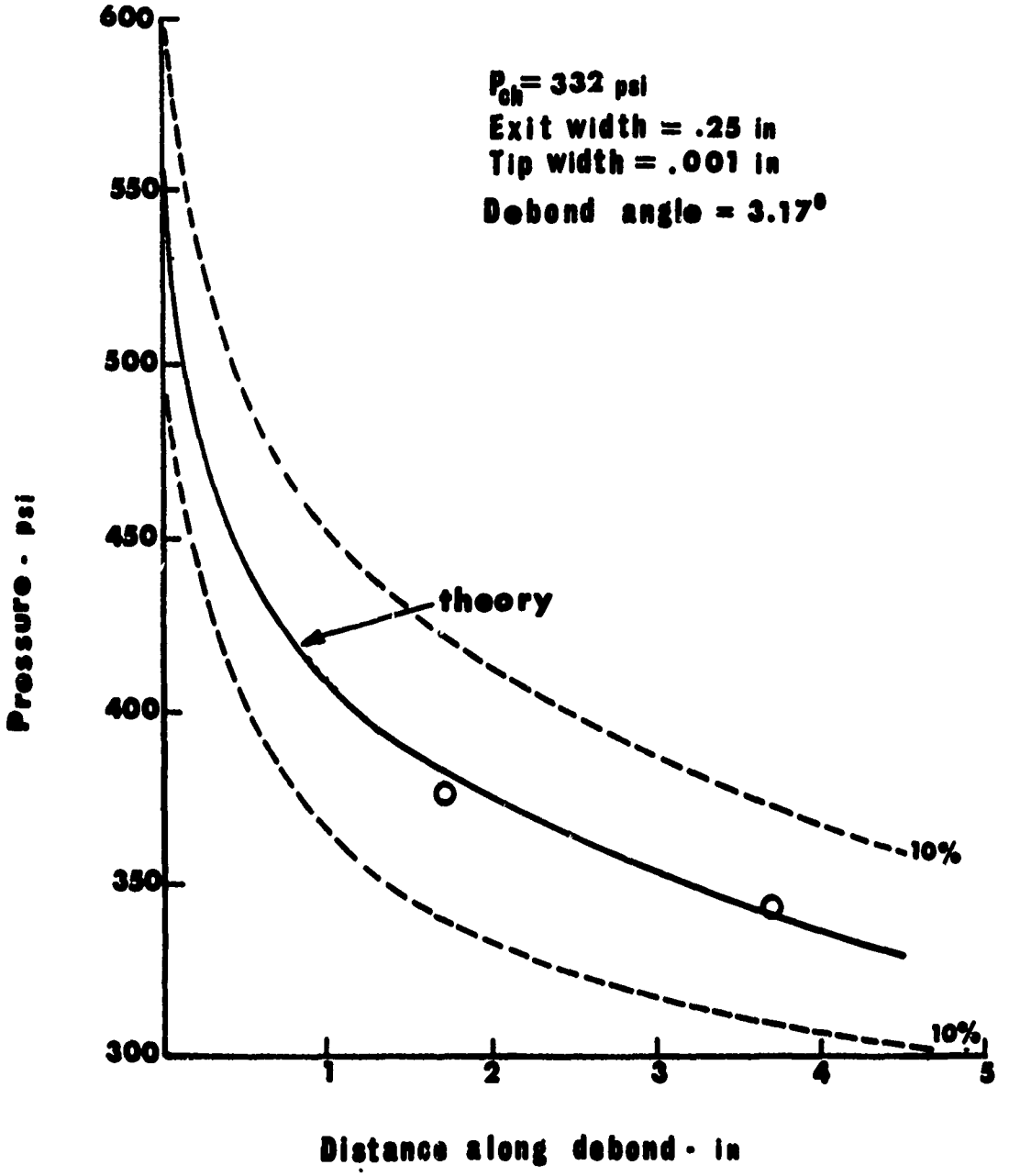

Figure 12 Pressure versus distance from tip

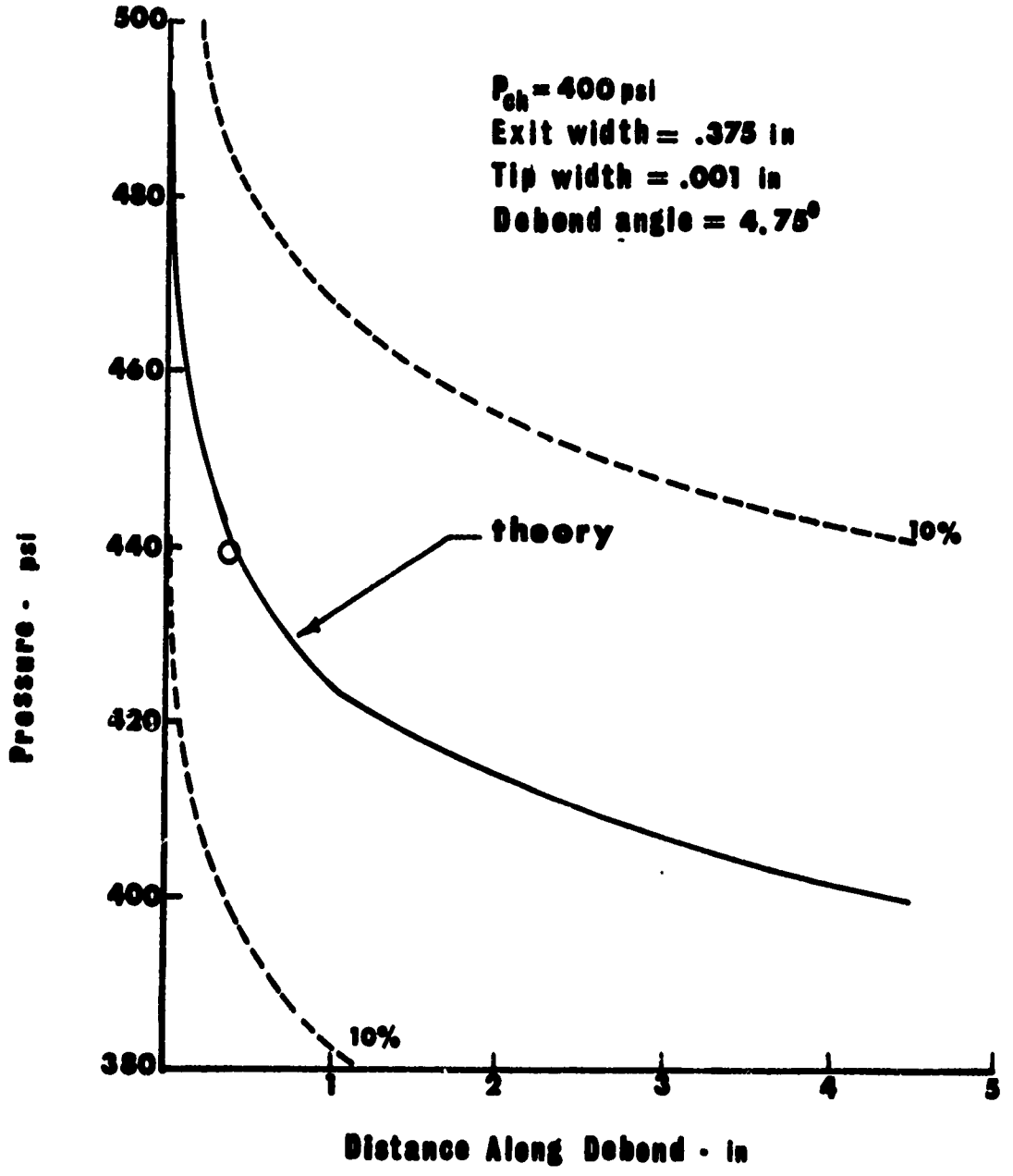

Figure 13 Pressure versus distance from tip

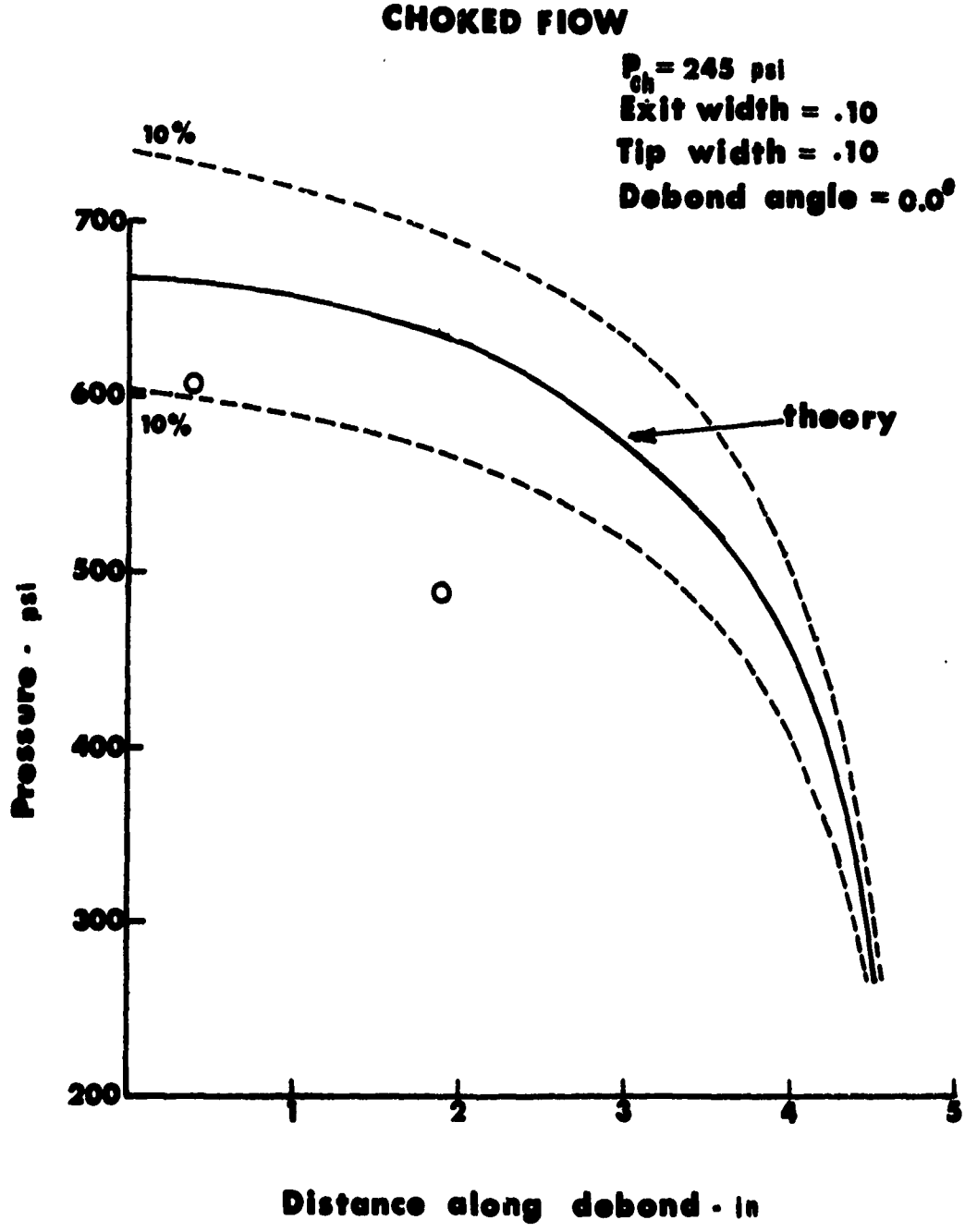

Figure 14 Pressure versus distance from tip

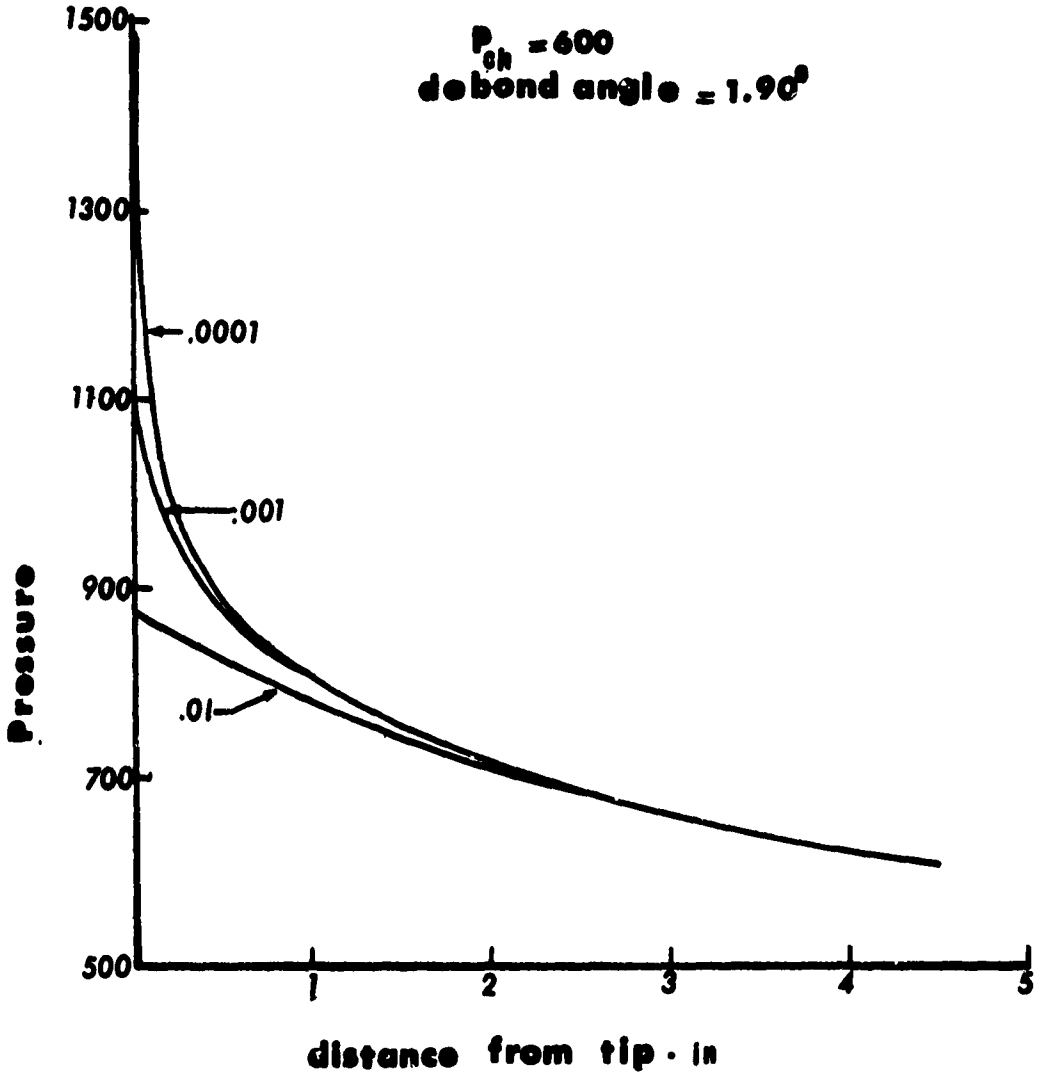

Figure 15 Effect of assumed tip width

from the tip. For points closer to the tip, the pressure will be somewhat affected by the tip width assumption. It can be seen from the figure that the changes induced in the debond pressure distribution by making the tip width smaller are limited to the immediate vicinity of the tip and that they approach the case where only the tip pressure itself is affected by a change in tip width. With this in mind and with some consideration of the increased computer time required for smaller tip widths, a tip width of 0.001 inches was chosen to be used in the theoretical predictions. Once the tip width was chosen, it was necessary to define the propellant properties.

The propellant utilized in these experiments is a double-based propellant loaded with aluminum. The parameters that are required for the analysis include burning temperature, burning rate coefficient, burning rate exponent, viscosity of gaseous effluent, propellant density, and the ratio of specific heats for the gaseous effluent (1, 2).

The data was reduced for each experiment by simply picking the chamber pressure for the case that was desired to be studied and then finding at which point the recorded chamber pressure trace crossed this value as long as the desired chamber pressure was reached in the first half second of the test. This latter restriction was placed on the experiment due to the fact that thermally induced drift exists in the pressure transducers. This technique of obtaining data at a specified pressure was also necessary due to the continuously changing chamber pressure. Values of pressure were read from the other three recorded traces at points corresponding to that of the desired chamber pressure. The one-half second limitation was also necessary to pick a chamber pressure in order to be sure that the burning had not changed the geometry appreciably.

Also, readings could not be taken too soon after the ignition switch had been thrown in order that stable burning might have time to establish itself. This limited the data that could be meaningfully reduced to that which occurred approximately between 0.20 and 0.5 seconds after ignition. The average time between electrical ignition contact and initial trace displacement was approximately 0.05 to 0.12 seconds. This delay was most likely due to heating of the ignition wire and also the time required for flow to begin moving outward from the debond after the surface had been ignited (see Figure 7). The delay encountered was very repeatable from one experiment to the next and lent itself to the accuracy of the instantaneous ignition assumption.

The data represented in Figures 10 and 11 was taken from the same four experiments. The data in Figure 10 for a chamber pressure of 550 psi was in the ideal range for data reduction as explained in the previous paragraph whereas the data in Figure 11 for a chamber pressure of 600 psi was taken at a later point after the chamber pressure had risen an additional 50 psi. A comparison of the error encountered in each case will yield larger errors for the case taken at the chamber pressure of 600 psi as compared to the one at 550 psi. This tells one that the error is increasing as the burning continues which is what would be expected due to the change in geometry. On the other hand, taking data too soon after ignition will yield even larger errors due to the uneven burning that occurs in the first 0.1 to 0.2 seconds after electrical ignition contact.

The data in Figures 8 and 9 were reduced from separate sets of experiments with each set of data being taken approximately between 0.20 and 0.3 seconds after ignition. The time required for the desired chamber pressure to be reached in each case varied due to inconsistancies in

the operation of the mechanical pressure relief valves.

As can be seen on any one of the graphs of experimental results, the number of data points is greatest near the exit, smaller near the center, and even smaller near the tip. The reason for this being that in some particular cases one of the channels would give either no output at all or would overscale completely. A galvanometer failure and this problem were responsible for the small number of points presented in each of Figures 12, 13, and 14. The channels that did function properly however, show very good agreement with the theory in every case.

An explanation of this behavior would be contaminants on the connectors or transducers themselves. With the extreme sensitivity to contaminants of these instruments as explained earlier the slightest bit of dirt or moisture would render the output meaningless. As for the increased frequency of bad data for the tip transducer, the explanation would be that the effect of contaminants must be a function of the charge output of the transducer or equivalently the magnitude of the pressure being measured. This seems reasonable on the basis that the contaminants act as stray capacitance in the line with the effect of this stray capacitance being dependent on the output of the transducer. Hence, the larger the output of the transducer, the larger the chance of the output being affected by contaminants. Also it was found later on in the experimental work that there were a few bad connections existing in the circuitry. These bad connections were of the type that would either work properly or not at all. Hence, there existed a possibility of a particular channel not working at all for any given test due to a loss of electrical contact. In some cases the contacts were good and a particular channel would fail to give a meaningful output due to other effects.

ERROR ANALYSIS

The average errors incurred in the experimental work varied from a low of approximately 0.1 per cent to a high of 19.8 per cent where average per cent error is taken to mean the difference between the theoretical prediction and the average of the experimental values divided by the magnitude of the theoretical prediction. A summary of the average errors encountered for some of the cases studied is given below.

Per Cent Average Error

Chamber Pressure, Psi	Tip	Center	Exit
170	5.5%	4.2%	0.1%
300	14.4%	10.8%	0.1%
550	11.4%	2.7%	2.1%
600	19.8%	2.2%	3.5%

Where the averages as shown above reflect reasonable errors in most cases, a considerable amount of scatter can be seen in the data especially in Figures 8 and 9 and the scatter is seen in increase for points close to the tip. The explanation for this behavior would most likely lie in the transducer and cables. As explained before contaminants could be responsible for this error.

The experimental procedure called for extreme care in attempting to keep the transducers and connectors clean. Freon T-F spray was used to clean the contact surfaces between each experiment and the inside of the pressure chamber was washed frequently. It is believed, however, that due to the large amount of contaminants produced by the burning, there is

little possibility of excluding these particles of dust or moisture from finding their way into the electrical contacts. The real problem arises after the burn is made and the connections between the low noise cable and the transducers are broken in order to remove the debond model from the bomb to be cleaned and recharged with new propellant. At this time the inside of the chamber iscompletely covered with combustion products from the burn including some moisture. With cautious preparation the effects of contaminants can be reduced somewhat but it is not reasonable, considering the large amount of material produced by burning, that their effect could be removed 100 per cent.

Contaminants could also have been responsible for errors in one other way. By inspection of the debond model after a burn it was noticed that deposits of a slag-like material had built up in small mounds on both sides of the debond, see Figure 16 and Figure 17. While these deposits present no problem to the flow nor will they affect the pressure distribution developed within the model, they do present a possible source of error in the readout. Although it cannot be substantiated, it seems possible that on certain runs the 1/16 inch connecting passages between the burning propellant and the transducers could be clogged or partially blocked by the buildup of this slag. This blocked passage would then be unable to transmit the pressure correctly and the output of the transducer would be in error. This then becomes another possible explanation for erroneous or incorrect data.

Experimental errors could have also developed from any one of several other factors along with those just discussed. For example, the burning rate law which is used in the mathematical analysis could be questioned somewhat. The burning characteristics of a solid propellant, particularly

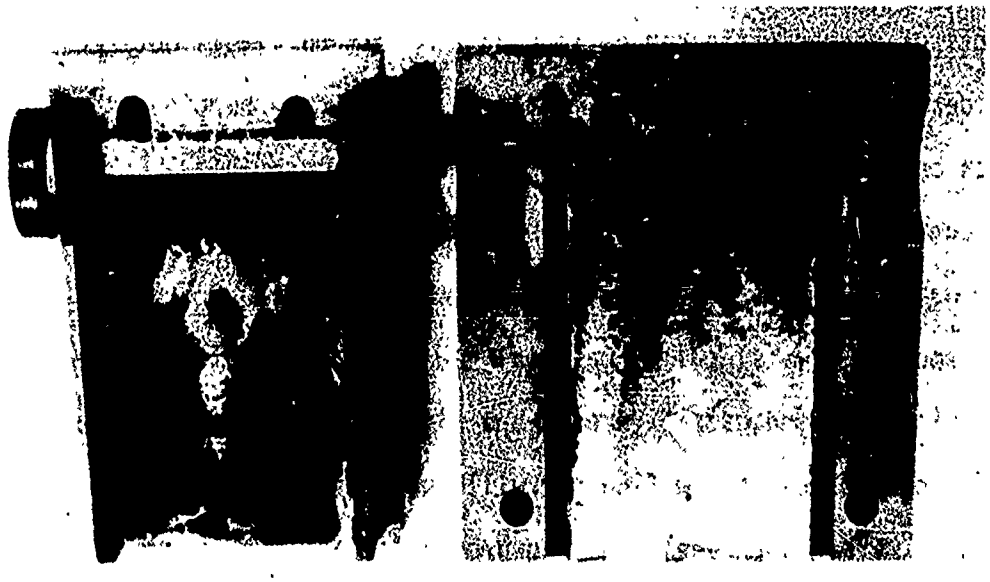

FIGURE 16. Debond model after a 3.17^{o} test

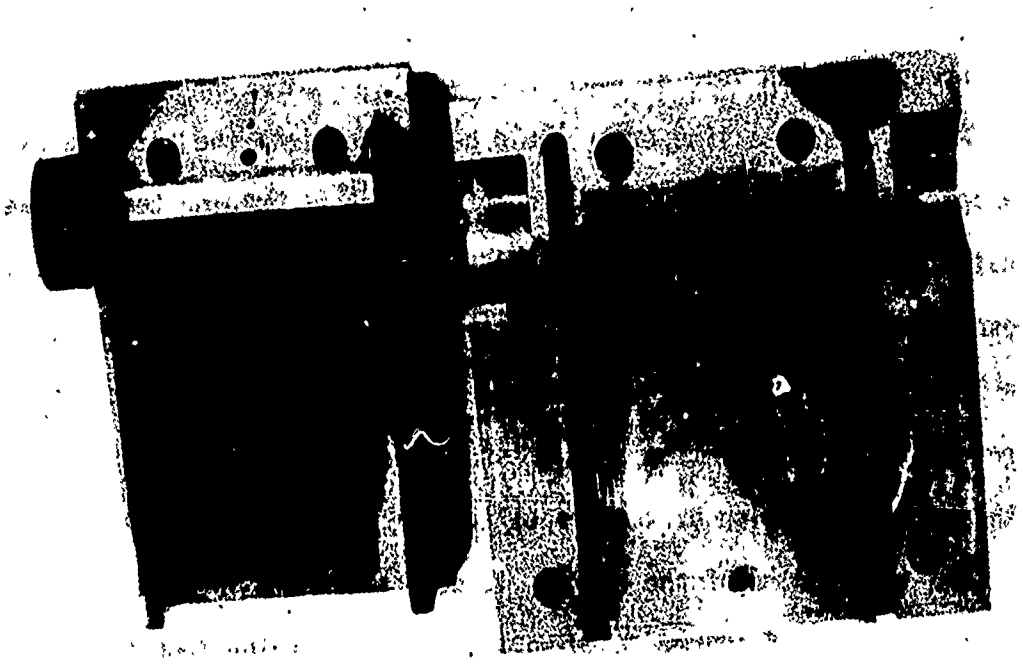

FIGURE 17. Debond model after a 4.75° test

TP-H1011, vary considerably with pressure. The burning rate law used here was arrived at experimentally by Thiokol engineers (1, 2) at a chamber pressure of about 724 psi. There is some question as to the exactness of this relation used for lower pressure ranges. Since it is believed that propellant of this type will burn with more stability at higher pressures, the burning rate law then becomes a possible source of discrepancy when used at lower pressures.

Along this same line, error could be induced into the analysis by the specification of propellant properties such as burning temperature, density, viscosity of effluent gases, and the ratio of specific heats. These properties vary generally from mix to mix and only average values can be specified. Where the burning temperature is more a function of the burning conditions, particularly pressure, the other properties can vary with age and condition of the propellant specimen. The analysis assumes that the temperature of the burning is constant where in reality it is a weak function of pressure. Knowing the correct burning temperature is a very important factor in the analysis.

That the burning is more stable at higher pressures can be seen in the reduction of scatter in the experimental data at the higher pressures compared to those at the lower chamber pressures. Also, since the burning rate increases with pressure, it is more likely that the ignition will occur in a more stable fashion at higher pressures. Countering the favorable effects of higher pressures is the fact that the increased burning rate makes the problem more transient in nature and the geometry more difficult to define after the burning has begun.

An additional difficulty in defining the initial geometry of the

debond is the variation encountered in the physical thickness of the propellant slab. The machining process used to cut the slabs could only guarantee a tolerance in thickness of $\pm$ 0.03 inches due to the viscoelastic behavior of the propellant while being cut. The effect of this variation in thickness along with the thickness of the layer of adhesive used to bond the propellant to the model beomces significant. The error induced by this variance in thickness increases as the angle of divergence of the debond decreases and errors of as high as ten per cent in the specification of geometry can be incurred due to this effect alone. The effect also will have larger magnitudes near the tip where a variance of geometry on the order of $\pm$ 0.03 inches can make as high as 100 per cent change in the debond width.

In Figure 16 a dark area can be seen which is approximately one inch wide and at the end of the model where the tip exists. This burn was made at an angle of 3.17 degrees and the dark area in question was a result of the propellant slab being thicker than 0.1 inches which caused the propellant to be in contact with the top surface of the debond completely covering the passage to the tip transducer. This caused a delay in the tip transducer's response for a time sufficient to allow burning to open up the crack and uncover the passage to the transducer. This drastic change in the geometry made this test less meaningful and the tip pressure totally meaningless. This effect was present to a lesser degree in other runs.

Two other possible sources of error were investigated to determine their contribution. These were possible temperature effects on the transducers and also the possibility of the effect of ionized gasses near the transducer. In order to determine if changes in the temperature of the transducer itself would effect the output, an acetlyene torch

was used to simulate the hot flowing gasses that exist in the debond while at the same time creating no appreciable pressures on the transducers. This test was made with the lower half of the debond model taken off so that the hot gasses could flow freely over the surface where the transducers were mounted. The test showed that there was little or no effect due to the existence of the hot gas but that there was some appreciable drift due to conduction through the plate to the transducer. This drift was on the order of an equivalence of 50 psi but did not occur until approximately two to three seconds after application of the hot torch. However, the 6000^{0}F temperature of combustion of the propellant within the debond could cause a larger drift. Thus, it was concluded that temperature effects due to conduction thru the plate although present in significant magnitude were not present during the critical test period of 0.5 seconds and therefore had no bearing on the test results.

To test for the effects of ionized gases the same test with the torch was conducted with the recessed cavity and connecting passage filled with bearing grease. This way no ionized gasses could come in contact with or get near the transducers. The results of the test were the same as those obtained with no grease in the recessed cavity and connection passage. Thus it could be concluded that ionized gasses had no effect on the output of the transducers.

If one studies the trend of the experimental results compared to the theory for the tip transducer it will become evident that experimental values lie above predicted values in most of the cases. If the assumed tip width were changed from .001 inches to .0001 inches a change in the predicted pressures near the tip would occur as seen in Figure 1 . This increase in the magnitude of the predicted values near the tip would

significantly reduce the variance between experimental and theoretical values. Thus the values of average error for the tip transducer as given earlier in this section are high and would be reduced significantly by use of a smaller assumed tip width. The data is left in terms of a tip width of 0.001 of an inch due to difficulty in the computer iteration scheme encountered when the tip is assumed smaller.

With some consideration of the large number of factors which contribute to the possibility of errors in the experimental data, the deviations that were encountered become of reasonable magnitude. Even the large amount of scatter that was seen in some cases seems reasonable given the factors which could cause behavior of this type. With all of the errors mentioned, there has as of yet been no mention of assumptions given in the theoretical analysis such as one-dimensional flow, etc. These assumptions could also make induced error. This consideration along with the experimental error analysis makes the results feasible on the basis of an engineering error analysis.

CONCLUSIONS

The experimental work conducted gives good substantiation of the pressure distribution in a debond as calculated using one-dimensional compressible flow theory. The cases studied cover a range of chamber pressures from 170 psi to 600 psi and a range of debond angles from 1.90 degrees of 4.75 degrees. The range of angles studied cover completely those angles allowed under the one-dimensional flow assumption and the chamber pressures cover the range of pressures allowed for safety by the experimental equipment.

It would be reasonable to conclude at this time that the analytical and numerical methods used here to predict pressure distributions in burning propellant debonds and cracks are valid for angles below approximately five degrees and chamber pressures in the range studied. Also there is good reason to believe that the results would compare more favorably for tests run at higher chamber pressures.

With a working method to predict pressures in flaws it is now possible to couple one-dimensional flow analyses with a study of the mechanical properties of propellants and predict when failure will occur due to an existing flaw in a solid propellant grain.

REFERENCES

1. Personal communication with S. John Bennett, Thiokol Chemical Corporation, Utah Division, Brigham City, Utah.

2. Personal communication with Garron P. Anderson, Thiokol Chemical Corporation, Utah Division, Brigham City, Utah.

3. United Technology Center, "Development of Non-Destructive Testing Techniques for Large Solid Propellant Rocket Motors." Contractor Report No. UTC 2015-FR, Air Force Contract AFO 4(611)-8018, Final Report. April 1963.

4. Hsiao, C. C. and Moghe, S. R., "Stress Field and Fracturing of Solid Propellants During Rocket Firing." AIAA Journal. 1, 363. August 1963.

5. Magnussen, B., "Radiographic Analysis of Defects in Solid Propellant Motors." Proceedings of BuWeps Missile and Rocket Symposium, NAD Concord. April 1961.

6. Payne, C. E., "Flame Propagation in Propellant Cracks." AFRPL-TR-69-66, Air Force Rocket Propulsion Laboratory. 1969.

7. Godai, T., "Flame Propagation into the Crack of Solid Propellant Grain." AIAA Paper No. 69-561, AIAA Fifth Propulsion Specialist Conference. June 1969.

8. Derbidge, T. C., "One-Dimensional Compressible Flow in a Variable Area Duct with Mass Addition." Unpublished master's degree thesis, Department of Mechanical Engineering, University of Utah, Salt Lake City, Utah. June 1970.

9. Gross, J. T., Hartnett, J. P., et al., "A Review of Binary Boundary Layer Characteristics." RM 2516, The Rand Corporation. June 1959.

10. Spalding, D. B., Audlander, D. M., and Sundaram, R. T., "The Calculation of Heat and Mass Transfer through the Turbulent Boundary Layer on a Flat Plate at High Mach Numbers, With and Without Chemical Reaction." Supersonic Flow, Chemical Processes and Radiation Transfer, D. B. Olfe and V. Zakkuy, ed. Oxford: Pergamon Press. 1964.

11. Nikuradse, J., "Gestzmassigkeiten der Turbulenten Stromung in Glasten Rohren." VDE-Forschungsh. 356, 21. 1932.

12. Price, E. W., "One-Dimensional Steady Flow with Mass Addition and the Effects of Combustion Chamber Flow on Rocket Thrust." Jet Propulsion. 1, 92. February 1955.

13. Kistler Instrument Corporation," Model 568 Universal Electrostatic Charge Amplifier Operating and Service Instructions." January 1963.

APPENDIX A

A listing of the computer program used to solve equations 20 and 24 numerically is given in this appendix. This program is a slightly revised version of the program developed in Reference 8. The basic solution technique is the same with changes occurring in some areas to make the program better fit the debond configuration being studied.

The program basically consists of two loops with the solution technique being an iterative procedure. The basic method which the program utilizes is that of initially quessing a tip pressure and then based on that guess the distribution of pressure within the entire debond is calculated. Once this is done the exit boundary conditions can be checked and a new value for tip pressure can be calculated based on the old value and the error encountered in the boundary condition check. The procedure is repeated until the boundary condition check and the proper distribution of pressure is found.

The basic object of having two such similar loops is that loop 1, in general, will differentiate the choked from the non-choked flows or in other words loop 1 attempts to match the boundary condition that P(N) = PC and V(N) = 1. The second loop basically takes care of choked flows i.e. V(N) = 1.

Table A-1 gives a comparison of the variables used in the computer program and the analyses. For a more detailed explanation of the program, a flow chart, and a listing that will handle cracks as well as debonds the reader should see Appendix B in Reference 8.

TABLE A1. Nomenclature and Units Used in Computer Program

Analysis	Computer	Units
Br	BR(I)	none
C	C	$ft^{2n+1}/sec\text{-}lbf^{n}$
D	D	lbm/ft^{3}
f	FC	none
G^2	F	$(sec\text{-}lbf/lbm)^{2}$
H	HBR	none
M	V(I)	none
n	XP	none
P	P(I)	psi
P_o	PO	psi
P_{ch}	PC	psi
$\bar{P}$	Z(I)	none
$\bar{P}'$	ZP	1/in.
R	R	$ft\text{-}lbf/lbm^{o}R$
R_e	RE(I)	none
T_o	TO	^{o}R
x	S(I)	in.
Δx	H	in.
y	Y(I)	in.
y'	YP(I)	none
γ	GM	none
ζ	X(I)	none
μ	U	$lbf/sec/ft^{2}$
η	T(I)	sec/ft
η_o	THO	none

```
      DIMENSION Y(2000),YP(2000),S(2000) ,Z(2000),X(2000),
     *     V(2000)
      DIMENSION P(2000),T(2000),RE(2000),BR(2000),JJ(3)
      REAL LL
    5 READ 3, YN,LL,PC,YO
      DATA DIF,ERROR,H,L,MAX/.01,1.,.01,10,100/
      N = 451
      NA=N
C*************************************************************C
C LL=DEBOND LENGTH                                            C
C YN=DEBOND EXIT WIDTH                                        C
C PC=CHAMBER PRESSURE                                         C
C YO=TIP WIDTH                                                C
C COMPUTER PARAMETERS                                         C
C DIF=ALLOWABLE ERROR BETWEEN ACTUAL MACH NO AND MACH 1.0     C
C ERROR=ERROR IN PRESSURE BETWEEN CHAMBER AND EXIT            C
C H=STEP SIZE IN INCHES                                       C
C L=NO OF STEPS PRINTED IE PRINT EVERY L TH STEP              C
C MAX=MAXIMUM NO OF ITERATIONS ALLOWED                        C
C N=NO OF STEPS TAKEN                                         C
C NA=NO OF STEPS PRINTED - IE NA STEPS                        C
C PROPERTIES OF TP-H1011 PROPELLANT                           C
C U=VISCOSITY  LBF SEC/FT**2                                  C
C C=BURNING RATE COEFFICIENT  FT**(2XP+1)/SEC LBF**XP         C
C D=PROPELLANT DENSITY  LBM/FT**3                             C
C TO=BURNING TEMPERATURE  R                                   C
C GM=RATIO OF SPECIFIC HEATS                                  C
C XP=BURNING RATE EXPONENT                                    C
C R=GAS CONSTANT  FT LBF/LBM R                                C
C*************************************************************C
      C=.0047
      TO=6200.
      D=111.
      XP=.25
      GM=1.1
      U=.00000202
      R=(1545.)/(28.28)
C             INPUT GEOMETRY FOR DEBOND
      S(1)=0.
      YP(1)=(YN-YO)/LL
      THETA=ATAN(YP(1))
      Y(1)=YO
  333 DO 2 II=2,N
      YP(II)=YP(1)
      S(II)=H*(II-1)
```

```
      Y(II)=YP(II)*S(II)+YO
    2 CONTINUE
      Y(N)=YN
C               PRINT HEADING AND DEBOND GEOMETRY
  998 PRINT 1 LL,Y(1),Y(N),PC
  999 NI=1
C INITIAL PO GUESS
      PO=PC+1
      PORS=PC
      SR=0.
      GO TO 26
   24 CONTINUE
      DPOS=PO-PORS
      DS=S(I)-SR
      IF(DS)100,101,100
  101 DS=H
  100 CONTINUE
      SR=S(I)
      PORS=PO
      IF(NI-6)54,54,53
   54 SDIV=10.
      GO TO 57
   53 IF (NI-10.)929,929,930
  929 SDIV=3.0
      GO TO 57
  930 SDIV=1.0
   57 CONTINUE
C CORRECTED PO GUESS
      PO=PORS+(DPOS/SDIV)*(S(N)-SR)/DS
   26 CONTINUE
      B=0.
      AA=(PO*144.)**(XP-1.)
      THO=D*C*AA
      T(1)=THO
      Z(1)=1.
      F=(2.*(GM-1.)*TO*R)/(GM*32.2)
      NI=NI+1
      IF(NI-MAX)58,58,29
   58 CONTINUE
      DO 36 I=1,N
      P(I)=PO * Z(I)
      IF(I-N)50,22,22
   50 CONTINUE
      IF(P(I)+ERROR-PC)24,22,22
   22 CONTINUE
```

```
      X(I)=SQRT(Z(I)*Z(I)+F*T(I)*T(I))
      V(I)=(X(I)-Z(I))/(Z(I)*(GM-1.))
      IF(I-N)51,23,23
   51 CONTINUE
      IF(V(I)-1.)23,24,24
   23 CONTINUE
      RE(I)=(Y(I)*T(I)*P0*24.)/(U*32.2)
      IF (RE(I) - 2200.) 20, 20, 21
C        FRICTION FACTORS FC ESTIMATED FROM REFERENCE 8
   20 FC=64./RE(I)
      GO TO 27
   21 IF (RE(I)-4000.) 400,400,401
  400 FC=.075
      GO TO 27
  401 FC=.07
   27 CONTINUE
      BR(I)=TH0*Z(I)**XP*SQRT(RE(I))/T(I)
   52 CONTINUE
      IF(N-I)108,108,105
  105 CONTINUE
      HBR=1./(2.*(BR(I)+1.))+1./(2.*5.**(BR(I)/4.))
      B2=F*T(I)/X(I)
      B4=(GM*X(I))/((X(I)-GM*Z(I))*Y(I))
      B1=(X(I)-Z(I))*(FC*(1.+HBR)/2.+YP(I))
      B3=TH0*Z(I)**XP-YP(I)*T(I)
      ZP=B4*(B1+B2*B3)
      Z(I+1)=Z(I)+H*ZP
      IF(Z(I+1)+Z(I))24,24,25
   25 CONTINUE
      B=(Z(I+1)+Z(I))**XP+B
      T(I+1)=(TH0/Y(I+1))*(H*B/2.**XP+Y0)
  108 CONTINUE
      V(I)=SQRT(V(I))
   36 CONTINUE
      IF(V(N)-DIF-1.)60,60,59
   60 IF(P(N)+ERROR-PC)90,56,91
   91 IF(ABS(P(N)-PC)-ERROR)56,56,92
   92 IF(ABS(V(N)-1.)-DIF)56,56,93
   93 IF(ABS(P(N)-PC)/PC-ABS(1.-V(N)))90,90,88
   59 DP0=P0/100.
      GO TO 89
   90 DP0=(PC-P(N))/10.
      GO TO 89
   88 DP0=P0/100.
   89 CONTINUE
```

```
      PO=PO+DPO
      EXUP=DPO/10.
      NV=1
      NP=1
   55 CONTINUE
      VR=V(I)
      PR=P(I)
      NI=NI+1
      IF(NI-MAX)86,86,29
   86 CONTINUE
      B=0.
      THO=D*C*(PO*144.)**(XP-1.)
      T(1)=THO
      Z(1)=1.
      DO 37 I=1,N
      F=(2.*(GM-1.)*TO*R)/(GM*32.2)
      P(I)=PO*Z(I)
      IF(I-N)61,62,62
   61 CONTINUE
      IF(P(I)+ERROR-PC)24,62,62
   62 CONTINUE
      X(I)=SQRT(Z(I)*Z(I)+F*T(I)*T(I))
      V(I)=(X(I)-Z(I))/(Z(I)*(GM-1.))
      IF(I-N)63,64,64
   63 CONTINUE
      IF(V(I)-1.)64,64,24
   64 CONTINUE
      RE(I)=(Y(I)*T(I)*PO*24.)/(U*32.2)
      IF(RE(I)-2200.)65,65,66
   65 FC=64./RE(I)
      GO TO 67
   66 IF (RE(I)-4000.)500,500,501
  500 FC=.075
      GO TO 67
  501 FC=.07
   67 CONTINUE
      BR(I)=THO*Z(I)**XP*SQRT(RE(I))/T(I)
      HBR=1./(2.*(BR(I)+1.))+1./(2.*5.**(BR(I)/4.))
      IF(N-I)106,106,107
  107 CONTINUE
      B2= F * T(I) / X(I)
      B4 = (GM* X(I)) / ((X(I) - GM * Z(I))*Y(I))
      B1=(X(I)-Z(I))*(FC*(1.+HBR)/2.+YP(I))
      B3=THO*Z(I)**XP-YP(I)*T(I)
      ZP=B4*(B1+B2*B3)
```

```
      Z(I+1)=Z(I)+H*ZP
      IF(Z(I+1)+Z(I))24,69,69
   69 CONTINUE
      B=(Z(I+1)+Z(I))**XP+B
      T(I+1)=(THO/Y(I+1))*(H*B/2.**XP+YO)
  106 CONTINUE
      V(I)=SQRT(V(I))
   37 CONTINUE
      DP=P(N)-PR
      DV=V(N)-VR
      DRC=ABS(P(N)-PC)/PC-ABS(1.-V(N))
      IF(P(N)+ERROR-PC)80,81,81
   81 IF(V(N)-DIF-1.)82,56,83
   82 IF(ABS(P(N)-PC)-ERROR)56,56,87
   87 IF(ABS(V(N)-1.)-DIF)56,56,84
   84 IF(ABS(P(N)-PC)/P(N)-ABS(1.-V(N)))80,80,83
   80 CONTINUE
      NP=NP+1
      CNP=ABS(DP/EXDP)
      IF(NP-2)95,95,94
   95 PDIV=3.
      GO TO 99
   94 PDIV=CNP
   99 CONTINUE
      POR=PO-((P(N)-PC)/PDIV)*DPO/DP
      EXDP=(P(N)-PC)/PDIV
      GO TO 85
   83 CONTINUE
      NV=NV+1
      IF(NV-2)97,97,96
   96 IF(ABS(V(N)-1.)-.3)104,103,103
  104 VDIV=2.
      GO TO 98
   97 IF(ABS(V(N)-1.)-.3)102,103,103
  102 VDIV=3.
      GO TO 98
  103 VDIV=10.0
   98 CONTINUE
      POR=PO-((V(N)-1.)/VDIV)*DPO/DV
   85 CONTINUE
      DPO= POR-PO
      PO=POR
      GO TO 55
   56 CONTINUE
  801 PRINT 7
```

```
      PRINT 8 (S(I),Y(I),P(I),V(I),I=1,NA,L)
C              PRINT PROPERTIES AT LOCATION OF TRANSDUCERS
C              IE .19  1.72 AND 3.72 INCHES FROM TIP
      JJ(1)=20.
      JJ(2)=JJ(1)+153.
      JJ(3)=JJ(2)+200.
      DO 300 KK=1,3
      K=JJ(KK)
      PRINT 8  S(K),Y(K),P(K),V(K)
  300 CONTINUE
      THETA=THETA*57.3
      PRINT 301 XP,R, U,C,D,GM,THETA
      GO TO 5
   29 CONTINUE
      PRINT 72
    1 FORMAT (1H1,54X,'DEBOND GEOMETRY',/,18X,
     *     'DEBOND LENGTH',13X,'TIP WIDTH',13X,'EXIT WIDTH',
     *      13X,'CHAMBER PRESSURE',/,21X,F5.2,20X,F6.4,15X,
     *     F6.4,20X,F6.1,/,)
    3 FORMAT (5F10.4)
    7 FORMAT (28X,'S(I) INCHES',9X,'Y(I) INCHES',11X,
     *      'P(I) PSI',13X'MACH NO.')
    8 FORMAT (28X,F10.4,10X,F10.4,10X,F10.2,10X,F10.4)
   72 FORMAT(' ',' ITERATION UNSTABLE')
  301 FORMAT (1H0,10X,'XP=',F4.2,3X,'R=',F4.1,3X,'U=',
     *       F10.  9,3X,'C=',F6.4,3X,'D=',F5.1,3X,'GM=',F3.1,
     *       3X,'CRACK ANGLE=',F4.2,1X,'DEGREES')
      END
```